Most azole antifungal resistance mutations in the drug target provide cross-resistance and carry no intrinsic fitness cost

Camille Bédard[1,2,3,4,5], Isabelle Gagnon-Arsenault[1,2,3,4,5], Jonathan Boisvert[1,3,4,5], Samuel Plante[1,2,3,4,5], Alexandre K Dubé[1,2,3,4,5,], Alicia Pageau[1,2,3,4,5], Jehoshua Sharma[6], Laetitia Maroc[6], Rebecca S. Shapiro[6] and Christian R Landry[1,2,3,4,5,]

1. Institut de Biologie Intégrative et des Systèmes (IBIS), Université Laval, G1V 0A6, Québec, Canada
2. Département de Biochimie, de Microbiologie et de Bio-informatique, Faculté des Sciences et de Génie, Université Laval, G1V 0A6, Québec, Canada
3. Département de Biologie, Faculté des Sciences et de Génie, Université Laval, G1V 0A6, Québec, Canada
4. PROTEO, Le regroupement québécois de recherche sur la fonction, l'ingénierie et les applications des protéines, Université Laval, G1V 0A6, Québec, Canada
5. Centre de Recherche sur les Données Massives (CRDM), Université Laval, G1V 0A6, Québec, Canada
6. Department of Molecular and Cellular Biology, University of Guelph, N1G 2W1, Guelph, Canada

Corresponding author: christian.landry@bio.ulaval.ca

Abstract

Azole antifungals are among the most frequently used drugs to treat fungal infections. Amino acid substitutions in and around the binding site of the azole target Erg11 (Cyp51) are a common resistance mechanism in pathogenic yeasts such as *Candida albicans*. How many and which mutations confer resistance, and at what cost, is however largely unknown. Here, we measure the impact of nearly 4,000 amino acid variants of the Erg11 ligand binding pocket on the susceptibility to six medical azoles. We find that a large fraction of amino acid substitutions lead to resistance (33%), most resistance mutations confer cross-resistance to two or more azoles (88%) and most importantly, only a handful of resistance mutations show a significant fitness cost in the absence of drug (9%). Our results reveal that selection for azole resistance can arise through a large set of mutations and this will likely lead to azole pan-resistance, with very little evolutionary compromise. Such a resource will help inform treatment choices in clinical settings and guide the development of new drugs.

Introduction

Antimicrobial resistance is a global development and health threat[1]. Drug resistance in fungi is particularly challenging because there is a very limited set of treatments to choose from, which means that treatment options are quickly exhausted when resistance mutations occur in patients[2]. Contrary to antibiotic resistance, antifungal resistance is not driven by the acquisition of genes but rather through mutations that occur *de novo* in the genome[3]. Accordingly, the mechanisms of resistance can be very diverse and difficult to predict.

Candida spp. are the main culprits of human fungal diseases, causing infections ranging from superficial to invasive. Opportunistic pathogenic yeasts are part of the microbiota of healthy people and are causing invasive diseases when the host immune system is compromised[4]. Among the species involved, *Candida albicans* is the most common cause of candidiasis[5] and it can lead up to 70% mortality when infections become invasive[4]. For these reasons and others, *C. albicans* has been classified as critical in the World Health Organization fungal pathogens priority list[6].

Candida infections are often treated with azoles[4,7,8]. Azoles target the cytochrome P450 lanosterol 14-alpha-demethylase (Erg11 in yeast and Cyp51 in molds), an important enzyme in the ergosterol biosynthesis pathway. When Erg11 is inhibited, ergosterol biosynthesis is blocked, which leads to the accumulation of a toxic sterol intermediate[9]. The evolution of resistance to azoles jeopardizes our ability to treat infected patients[10]. The widespread use of these molecules for treatment or as prophylaxis has led to the emergence of less susceptible isolates[11]. Amino acid substitutions in Erg11 are a common resistance mechanism in most *Candida* spp.[12,13] Resistance mutations can occur during treatment[2] and can lead to resistance against multiple azoles simultaneously, a phenomenon known as cross-resistance[3]. Resistance to azoles is not restricted to yeast infections as these drugs are also used to treat other fungal infections such as the ones caused by *Aspergillus spp*. The fact that azoles are also used in agriculture may further exacerbate the resistance problem as resistance mutations are selected in nature, even before fungi infect humans[14–16].

The evolution of antimicrobial resistance results from mutations that confer an advantage during treatment. An important factor that dictates the fate of resistance mutations is whether they reduce fitness in the absence of drugs, for instance following treatment interruption or spatial and temporal concentration heterogeneities[17,18]. Mutations with no or low costs are more likely to persist in populations in the absence of drugs, which can influence resistance management strategies[19]. Because antifungal drugs target essential genes or cellular processes, one could expect that resistance mutations would typically alter important protein functions and thus lead to significant fitness costs. Indeed, fitness tradeoffs linked to different resistance mechanisms have been characterized for all clinical antifungal classes[20–23]. Since lanosterol enters the catalytic pocket in Erg11 where azoles also do, one could expect a strong tradeoff for azole resistance mutations. Amino acid substitutions altering azole binding would also impair

lanosterol binding and demethylation. However, studies have shown that certain *ERG11* resistance mutations are not costly. For example, the amino acid substitution G464S, which is often observed in clinical resistant isolates of *C. albicans,* does not lead to any growth defect in the absence of drugs, at least in the laboratory[24]. The same has been observed for substitutions G54W and M220K in Cyp51A of *Aspergillus fumigatus*[25]. However, these observations could be biased since resistance mutations that are not costly are more likely to be sampled and isolated in the laboratory. Accordingly, we do not have a clear picture of the extent of fitness cost to azole resistance due to mutations in *ERG11*.

The number of antifungal resistance mutations inventoried in the literature is relatively small compared to all possible antimicrobial resistance mutations and, most importantly, only rarely has the causal link between the mutation and its resistance profile been experimentally validated[12]. Therefore, our knowledge about resistance mutations is insufficient to confidently predict if an amino acid change in Erg11 is going to lead to resistance or not, and what would be the cost associated with these mutations. There is a need for a comprehensive assessment of resistance mutations. Specifically, a better and more comprehensive understanding of the molecular mechanisms underlying resistance, cross-resistance and the associated tradeoffs would enable a better interpretation of the functional significance of *ERG11* genetic variants in *Candida* spp. genomes. Genomic tools could be useful to detect and monitor resistance mutations in a pathogen infecting a patient in real time throughout treatment, allowing for the adjustment of therapeutic use prior to treatment failure[26–28]. Another benefit from such knowledge would be to potentially modify current drugs to overcome or prevent resistance. For instance, a complete map of the resistance mutations in the binding pocket of a target would enable the rational design of drugs that specifically bind the resistant variants or that enter the pocket independently of the mutated residues[29]. Knowledge of resistance mutations would enable the development of effective drugs against resistant isolates without the need to discover completely new molecules or new target genes, which is a limiting factor for fungi because of their shared genes with humans. Finally, there is a large body of research currently attempting to find molecules that would potentiate existing antifungals or re-sensitize fungi to the drugs[30]. A better understanding of resistance mutations and their associated costs would allow us to strategically and rationally identify potentiators. The development of potentiators involves directing efforts towards pathways indirectly implicated in resistance, which are rendered vulnerable by the tradeoffs coming with resistance mutations. For all of these reasons, we aimed to comprehensively identify mutations imparting resistance to azoles, in and around their binding pocket in the enzyme Erg11 from *C. albicans*.

Pathogenic fungi are not easy to manipulate genetically. Methods have been developed and improved[31] but it is still challenging to engineer a large number of trackable mutants. However, studies have shown that *ERG11* from pathogens can be expressed in the model yeast *Saccharomyces cerevisiae* and complement *ScERG11*'s loss of function, enabling the assessment of the function and resistance of mutations in this model[32–38]. We thus constructed the largest set of Erg11 mutations to date, with nearly 4,000 mutants of *C. albicans* expressed

in *S. cerevisiae* engineered to act as a reporter for Erg11 activity. We competed all variants in parallel in the presence of six different azoles to measure resistance to individual drugs and cross-resistance, and in the absence of azole to assess the cost of mutations on the protein function. Our experiments allowed a thorough characterization of the protein variants leading to an extensive atlas of experimentally validated resistance mutations. Further analysis revealed that most azole resistance mutations in *ERG11* provide cross-resistance to azoles and carry no fitness cost. In addition to recovering previously reported high-confidence *CaERG11* resistance mutations, we validated one novel mutation in *C. albicans* by editing *ERG11* directly in its genome.

Results

Heterologous expression system

As *ERG11* is an essential gene in *S. cerevisiae,* we engineered a yeast strain to make *ScERG11's* expression repressible so it can be switched off on demand. We constructed a yeast strain with the *ERG11* promoter replaced with a doxycycline repressible one (*ScERG11*-DOX)[39]. This promoter is fully activated in the absence of doxycycline. In the presence of doxycycline, *ScERG11* is repressed enough to completely prevent growth. The expression of *CaERG11* from a plasmid rescues *ScERG11*-DOX growth in doxycycline medium, validating that *CaERG11* complements the *ScERG11* function in this context (Fig. 1a, Extended Data Fig. 1).

CaERG11 deep mutational scan

Since most amino acid substitutions known to confer resistance are found in regions adjacent to the enzyme's active site[7,40], we concentrated our efforts on residues most likely to perturb interactions with azoles. We examined the protein structures to find residues close to the ligand binding pocket. All the residues selected are located at less than 12 Å either from the lanosterol, fluconazole, itraconazole and heme molecules in the protein (Extended Data Fig. 2a). This range was chosen to include all well-characterized resistance mutations, including those further away from the ligand binding site such as Y257H (11.80 Å)[37,38,41–44] (Extended Data Fig. 2b).

The structural analysis led to a selection of 206 positions for the variant library (Fig. 1b, Extended Data Fig. 2c,d, Supplementary data 1). The library was designed to include the wild-type sequence and all 206 residues individually replaced by the 19 other amino acids. We used two codons per amino acid to improve data quality, except for methionine and tryptophan that are encoded by a single one (Supplementary data 2). *CaERG11* variants were synthesized and cloned into a plasmid containing the native promoter and terminator of *ScERG11* to ensure that expression regulation is similar to that of the native gene. We divided *CaERG11* into four overlapping sections to have DNA fragments of suitable size for high-throughput sequencing and we pooled the variants according to the fragment where their mutation is (Fig. 1b). We

transformed all plasmids into the *ScERG11*-DOX strain. The final library contains 3,830 amino acid variants (Extended Data Fig. 3).

We competed the variants with and without an azole to assess resistance and the fitness cost of mutations (Fig. 1c, Extended Data Fig. 4). We selected six azoles that are used in clinics and that have different structures. Fluconazole and itraconazole are first-generation triazoles, and their second-generation counterparts, voriconazole and posaconazole have similar chemical structures. Isavuconazole is one of the newest triazole. Clotrimazole is an imidazole widely used to treat superficial infections[45] (Fig. 2a). The concentration inhibiting around 50% of wild-type growth (IC_{50}, Extended Data Fig. 5) was used for the pooled competition assays in each case.

We measured variant frequencies by high-throughput sequencing at the start and the end of the eight generations of cell competition. Variant sequence coverage was higher than 700x on average per sample at the initial and final time points, providing high-quality data. The difference between the initial and final frequencies was used to calculate a selection coefficient (s) of all amino acid variants (Fig. 2b-h). The measurements were highly reproducible, with Spearman's rank correlation coefficient (ρ) among replicates ranging from 0.95 to 0.99 and for comparison within fragment overlaps ranging from 0.98 to 1.0 ($P < 0.0001$, Extended Data Fig.6 and 7). The selection coefficients of synonymous codons for each given amino acid were also strongly correlated (ρ between 0.92 and 0.98, $P < 0.0001$, Extended Data Fig. 8). The range of selection coefficients varies among azoles, but they all have similar distribution shapes (Extended Data Fig. 9).

We used the selection coefficient estimates (s) of individual amino acid variants to infer their resistance to azoles. We classified the variants into three categories: beneficial, deleterious and neutral (Fig. 1d). We performed a *t*-test to assess whether s estimates of missense variants were significantly different from that of the wild-type sequence. We defined variants as beneficial or deleterious if the *p*-value adjusted for false discovery rate (FDR) was lower than 0.01.

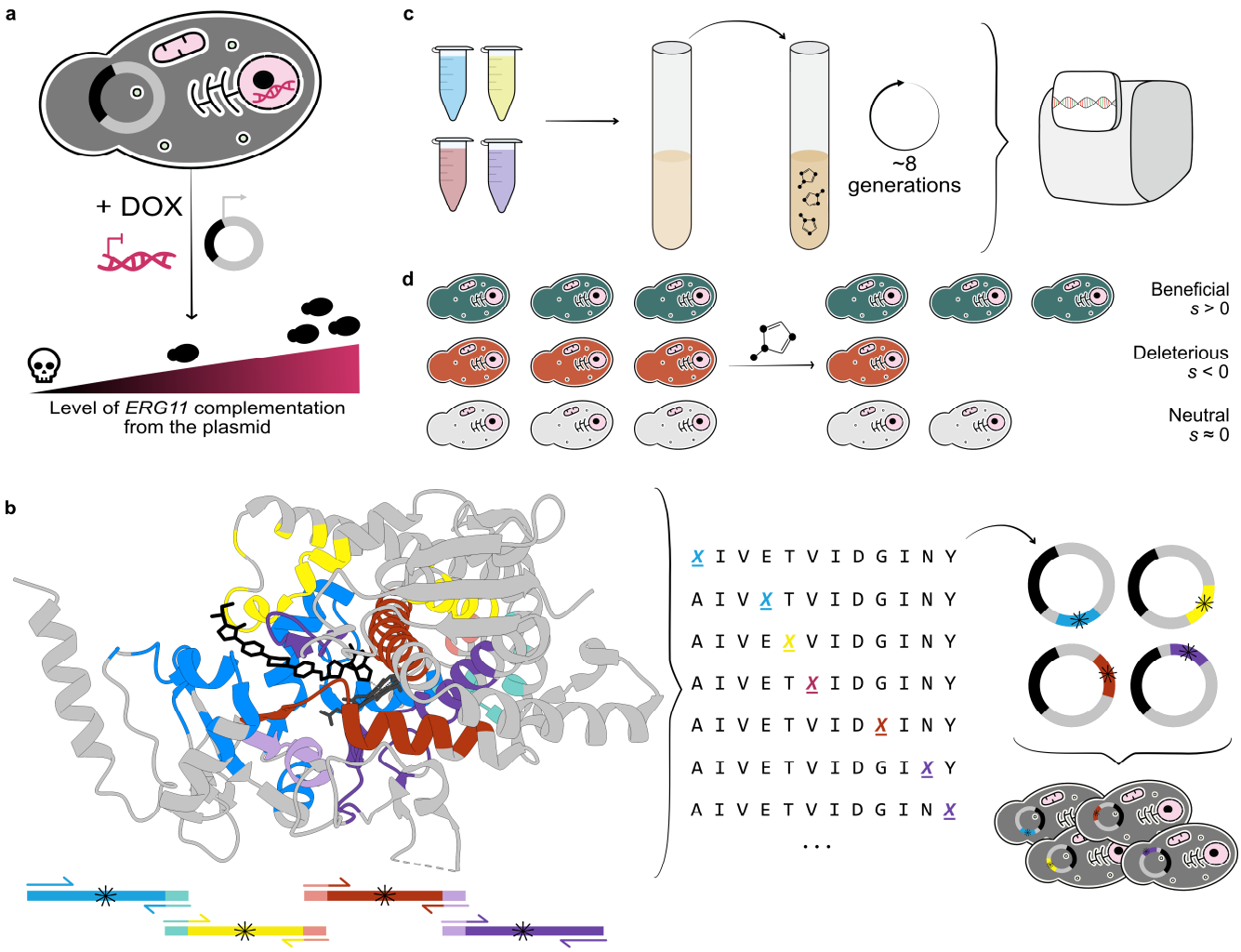

Fig. 1 | Experimental system for the systematic identification of azoles resistance mutations in their drug target Erg11. a, *CaERG11* heterologous expression system in *S. cerevisiae* (*ScERG11*-DOX). We replaced the endogenous promoter of *ScERG11* with a doxycycline (DOX on the figure) repressible promoter that is fully activated in the absence of doxycycline. When doxycycline is added to the culture medium, *ScERG11* is repressed, which prevents growth. A plasmid expressing *CaERG11* rescues *ScERG11*-DOX growth. **b,** Tertiary structure of CaErg11 bound to itraconazole (Protein Data Bank (PDB): 5V5Z) and mutagenesis. Colored residues were systematically mutated to all alternative amino acids. The library was split into four overlapping fragments to allow sequencing with short reads. The variant library was cloned into plasmids containing the native *ERG11* promoter and terminator of *S. cerevisiae* and transformed into the strain *ScERG11*-DOX. **c,** Pooled competition assays. The yeast library was pooled by fragments and grown without any selection pressure. Then, it was transferred into a medium containing doxycycline and an azole, and cells were left to compete for eight generations. Variant abundance at the beginning and at the end of the competition was estimated by high-throughput sequencing. **d,** Selection coefficient (*s*) to phenotype. Variant abundance before and after the competition was used to calculate selection coefficients. Variants were classified into three categories: beneficial, deleterious and neutral.

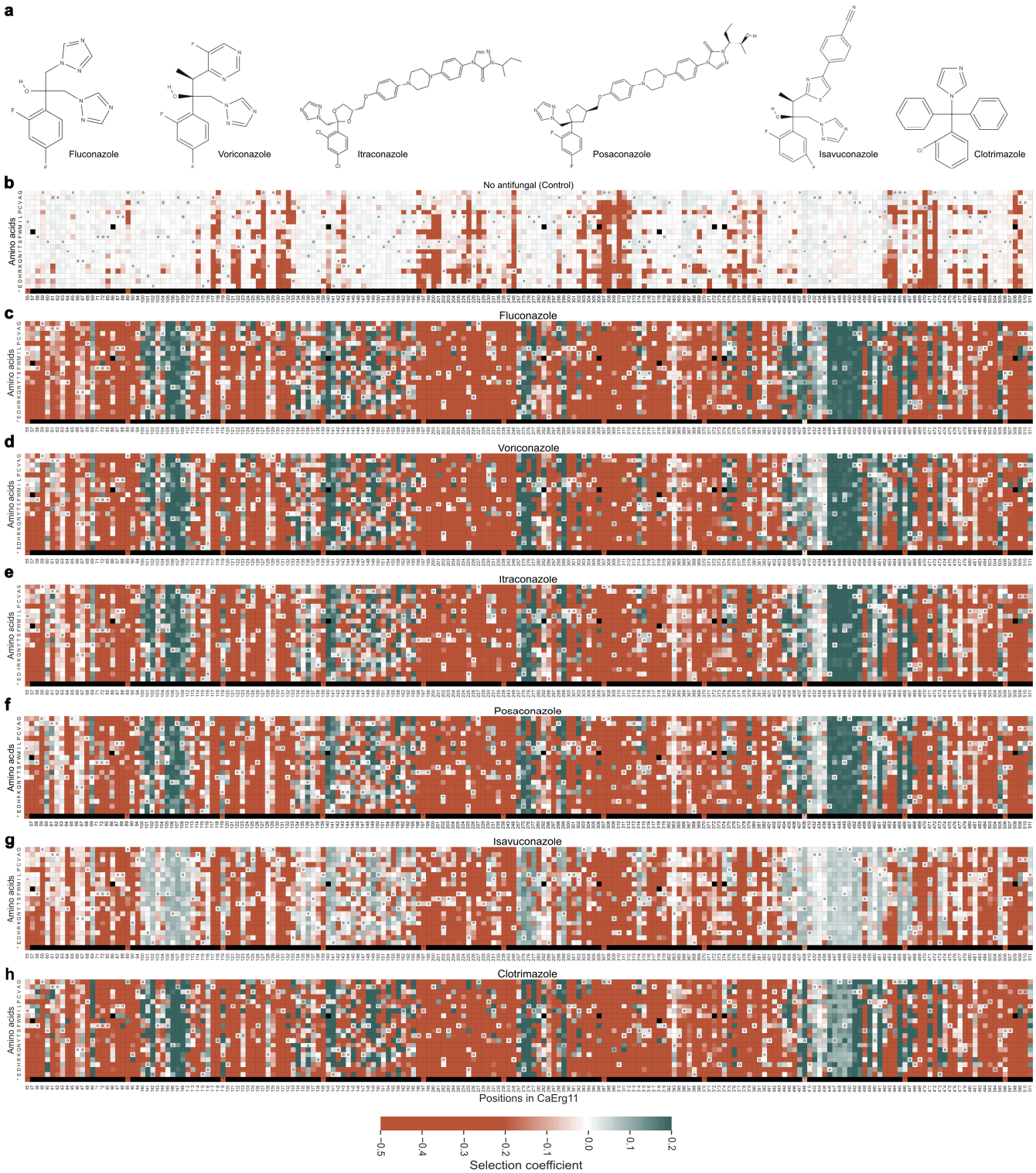

Fig. 2 | The resistance landscape of *C. albicans* Erg11 to six clinical azoles. a, Chemical structures of the azoles used. Structures were retrieved from PubChem[46]. **b,c,d,e,f,g,h,** Selection coefficients (s) of CaErg11 variants in control condition (**b**) and in fluconazole (**c**), voriconazole (**d**), itraconazole (**e**), posaconazole (**f**), isavuconazole (**g**) and clotrimazole (**h**). $s > 0$ (green) indicates higher fitness than the wild-type and $s < 0$ (orange) indicates lower fitness than the wild-type. "o" represents wild-type amino acids and * represents stop codons (stop codons were introduced as controls at every 20 residues). n = 3,830 amino acid variants. Each value is the median

170 of two synonymous codons per amino acid (in most cases), and triplicate experimental measurements. Black cells
171 represent missing values (wild-type amino acids tryptophan and methionine do not have synonymous codons).

Impact of mutations on the function of Erg11

172 We first focused on the impact of mutations on growth in the control condition (without azole).
173 As expected, the stop codons included as controls are highly deleterious (bottom row of
174 heatmaps in Fig. 2b-h). Not surprisingly for an essential enzyme, some mutations are as
175 deleterious as stop codons. Mutations that completely abolish the enzyme function form
176 clusters along the sequence (Fig. 3a). Positions near residues forming a hydrogen bond with
177 the heme (Y118, Y132, K143, R381, H468 and C470) and near residues participating in proton
178 transport to the heme (D225, H310 and T311) are the most sensitive to amino acid changes[47].
179 These positions are usually highly conserved among fungal orthologs, which validates their
180 important role in Erg11 canonical enzymatic reaction, more specifically in lanosterol
181 demethylation (Fig. 3b, Extended data Fig. 10).

182 To further validate our measurements, we examined the relationship between long-term
183 evolutionary constraints on the enzyme and the impact of mutations on fitness measured here.
184 We ran a mutational simulation using patterns of evolution of individual positions among
185 orthologs as implemented in GEMME[48]. The selection coefficients measured in the control
186 condition show a highly significant positive correlation with the evolution-based predictions (ρ
187 $= 0.40$, $P < 0.0001$). Interestingly, we observed fewer deleterious mutations than what GEMME
188 predicts (Extended Data Fig. 11a). One reason for the discrepancy between the predictions
189 and the measurements could be that there were recent changes in structure or function of
190 Erg11 that failed to be captured by comparing very distant orthologs. The experimental
191 conditions used here also do not reflect all the conditions this enzyme could have been selected
192 to perform in. In addition to altering the enzymatic activity, one other reason why mutations
193 could be deleterious for the function of Erg11 is destabilization. We therefore used FoldX[49] to
194 predict the effects of all amino acid substitutions on CaErg11 stability. We observed a negative
195 correlation ($\rho = -0.27$, $P < 0.0001$) between the change in free energy ($\Delta\Delta G$) predicted with
196 FoldX and s. This correlation suggests that some amino acid substitutions are deleterious
197 because they destabilize the enzyme, but it is likely not the only factor (Extended Data Fig.
198 11b).

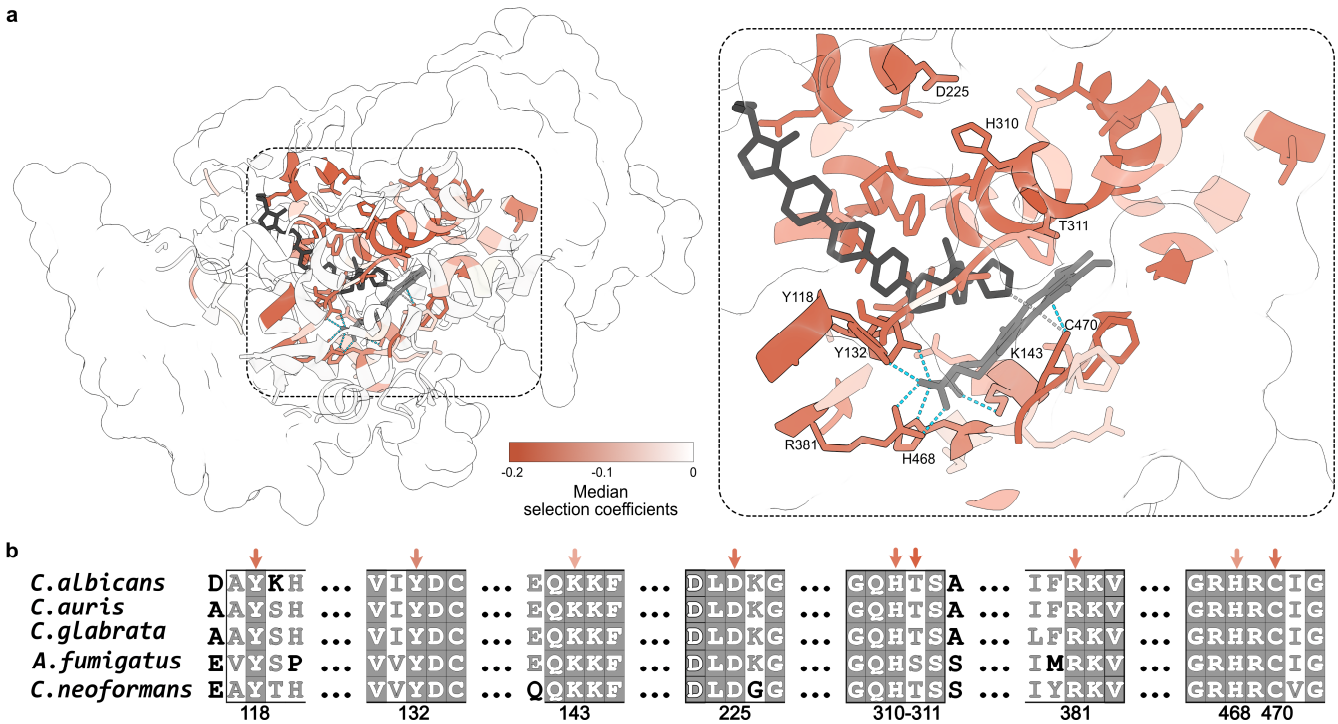

Fig. 3 | Mutations impairing CaErg11 canonical function are clustered and occur at conserved sites. a, Median selection coefficients in the control condition (without azole) mapped on CaErg11 bound to itraconazole (PDB ID : 5V5Z). On the right, only positions with deleterious variants are shown for clarity. Hydrogen bonds are represented as cyan dotted lines, itraconazole is in dark grey and heme molecule is in light grey. **b,** Multiple sequence alignment of Erg11 for some fungal pathogens listed on the WHO priority list (*Candida albicans*, *Candida auris*, *Aspergillus fumigatus* and *Cryptococcus neoformans*)[6]. Sequence is reduced to highlight conserved amino acids interacting with the heme (Y118, Y132, K143, R381, H468 and C470) and participating in proton transport to the heme (D225, H310 and T311). The complete alignment is available in Extended data Fig. 10 and was produced with ENDscript 2[50].

A large fraction of mutations lead to resistance, including outside of known hotspots

Through the analysis of selection coefficients, we identified a large number of mutations that significantly increase growth rate compared to the wild-type when cells are exposed to antifungals ($s > 0$, $P < 0.01$). We defined all variants with a $s > 0$ as beneficial when exposed to azoles, and thus resistant, even if resistant variants present a wide range of fitness. We identified 946 resistance amino acid substitutions for fluconazole, 1,044 for voriconazole, 999 for itraconazole, 1,011 for posaconazole, 1,009 for isavuconazole and 882 for clotrimazole, for a total of 5,891 mutation-resistance association.

We compared our results with known, experimentally validated resistance mutations in CaErg11. Since *C. albicans* is often subjected to treatments with fluconazole, mutations have been reported and validated experimentally for this particular drug. Amino acid substitutions A114S, T123H, Y132F, Y132H, K143E, K143Q, K143R, F145L, Y257H, S405F, D446E, G448E, F449V, G450E, Y447H, G464S and V456I have all been validated to confer at least a 2-fold decrease in fluconazole susceptibility[37,38,41–44]. All these mutants were classified as resistant in our experiments (s = 0.07 to 0.46), except for A114S which was categorized as

222 neutral, although it has a slightly positive *s* that is non-significant after correction for multiple
223 testing ($s = 0.04$, $P = 0.13$). Voriconazole and itraconazole are also often used to test for azole
224 susceptibility. Substitutions A114S, T123H, Y132F, Y132H, K143Q, K143R, F145L, Y257H,
225 S405F, G448E, G450E and G464S have been shown to confer a minimum 2-fold decrease in
226 voriconazole and itraconazole susceptibility in at least one study[37,38,41,42]. We classified mutants
227 carrying these substitutions as resistant to voriconazole ($s = 0.08$ to 0.47) and itraconazole (s
228 $= 0.07$ to 0.26), validating that the mutations indeed reduce susceptibility, contrary to what has
229 been reported in some other studies for voriconazole[41]. We provide the selection coefficients
230 and the classification for each CaErg11 variant as a resource (Supplementary data 3).

231 It has been proposed that resistance mutations cluster into three hotspots[51] based on
232 fluconazole and itraconazole resistant clinical isolates. The first hotspot extends from residue
233 105 to 165, the second from 266 to 287 and the third from 405 to 488. Since then, these
234 hotspots have been used as a reference in numerous papers to help interpret the impact of
235 mutations. In our experiments, we identified resistant mutants in the three clusters, as well as
236 at positions outside. More precisely, residues with more than 10 variants conferring fluconazole
237 resistance mostly fall into the hotspots (Extended data Fig.10). To visualize on the 3D protein
238 structure where the residues that most often confer resistance when mutated are located, the
239 medians of the selection coefficients were mapped on CaErg11 structure (Fig. 4a). We found
240 that the variants included in the hotspots form altogether a large cluster. However, if we instead
241 mapped on the structure all positions with at least one resistant variant (maximal values of *s*
242 per residue), we discovered that there are many resistant variants occurring outside the initial
243 clusters (Fig. 4b). We determined that 11% of the variants located outside the hotspots
244 (237/2078) confer fluconazole resistance, while 60% of those inside the hotspots remain
245 sensitive to azoles (1043/1752). In the light of these results, we believe that resistance hotspots
246 should be used with caution as a guide to interpret the impact of mutations in Erg11 since they
247 could potentially lead to inaccurate predictions of resistance.

248 We validated the impact of several mutations by reconstructing individual mutants by site-
249 directed mutagenesis of the wild-type *CaERG11* plasmid and by re-assessing the growth of the
250 variants individually. To do so, we constructed 35 variants covering a wide range of *s* in all
251 conditions. The variants were grown for 24h in media containing the azoles tested in the pooled
252 competition assays and in the control condition. The correlation between the growth of the
253 mutants and *s* in azoles is strong and highly significant (ρ ranging from 0.83 to 0.89, $P < 0.0001$),
254 showing that the high-throughput pooled assays are highly reproducible with individual mutants
255 on smaller scales (Fig.4c). Most variants in the control condition grew similarly, as anticipated.

Validation of a new resistance mutation in *C. albicans*

256 The experimental system we used is based on heterologous expression of the *CaERG11* gene
257 in *S. cerevisiae*. To validate the effects of a newly identified resistance mutation directly in *C.*
258 *albicans*, we used CRISPR-Cas9 to edit its genome. The strain we engineered is heterozygous

for H468T because editing efficiency is not high enough to edit both gene copies. As expected, the H468T strain grew better than the wild-type on fluconazole medium (Fig. 4d). It shows that resistance mutations we identified in *S. cerevisiae* by expressing a single allele appear to be at least partially dominant in a diploid genome. This would be an important aspect of resistance to be selected for, as resistance mutation that would be entirely recessive would not be visible to selection in a diploid species. We note however that loss of heterozygosity (LOH) is a frequent mechanism of resistance in *Candida spp*. such that heterozygous resistance mutations could rapidly become homozygous[52].

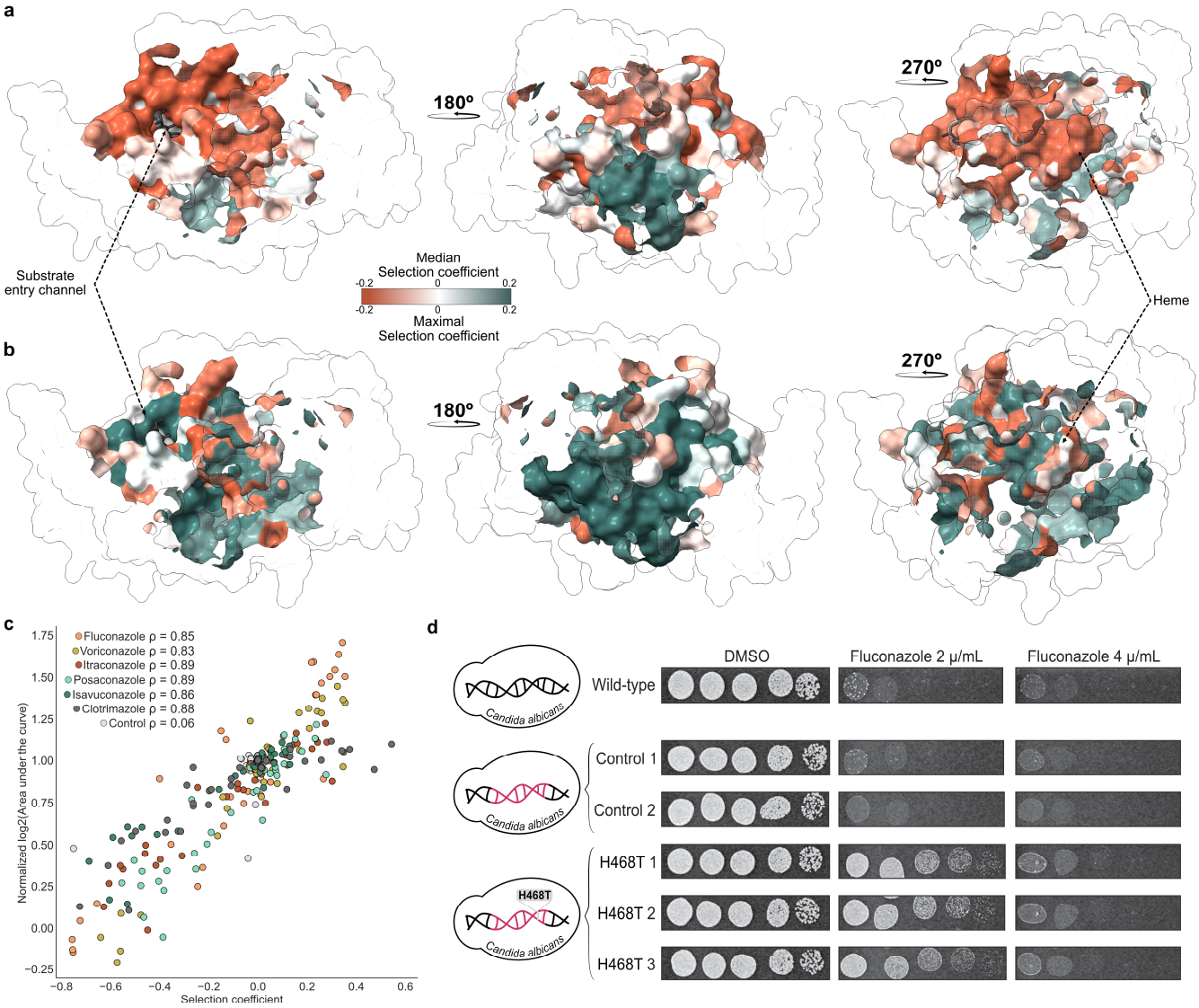

Fig. 4 | Azole resistance mutations in CaErg11 are scattered across the structure. a, CaErg11 (PDB ID 5V5Z) with the median selection coefficients per residue mapped on the structure. On the 180° rotation, a distinct cluster of residues showing strongly positive selection coefficients includes residues located in the three hotspots proposed by Marichal *et al.*[51] **b,** CaErg11 (PDB ID 5V5Z) with the maximal selection coefficients per residue mapped. We can see that resistance mutations are scattered across the structure and not limited to a single cluster. **c,** Validation of 35 variants individually reconstructed. Growth of mutants measured as Log2 of the area under the curve compared with the selection coefficient of the DMS competitions with and without azoles. The

values were normalized relative to the wild-type. Colors represent the different conditions. Each point is the average of two replicates. Spearman's rank correlation is shown, $P < 0.0001$. **d,** Spot assays of Erg11 H468T CRISPR-Cas9 genome edited *Candida albicans* compared to Erg11 wild-type CRISPR-Cas9 genome edited controls and SC5314 wild-type strain. Serial 1/5 dilutions of cells starting at an OD_{600} of 1 on YPD medium supplemented or not with fluconazole.

Most resistance mutations provide cross-resistance

Despite the fact that azoles have different structures, the patterns of resistance along the sequences appear to be strikingly similar (Fig. 2b-h). Indeed, selection coefficients are strongly correlated among azoles, with Spearman's rank correlation coefficients ranging from 0.93 to 0.99 ($P < 0.0001$, Extended Data Fig. 12). We found the strongest correlation between itraconazole and posaconazole ($\rho = 0.99$) followed by isavuconazole and itraconazole or posaconazole ($\rho = 0.97$). Fluconazole and clotrimazole were the least correlated to others ($\rho =$ 0.93 and 0.94), except for the fluconazole-voriconazole pair ($\rho = 0.96$). These correlations do not reflect the overall similarities among the molecules. The specificity of azoles may therefore derive from subtle differences in interactions between the molecules and CaErg11.

Overall, 33% (1,268) of the amino acid changes tested confer a significant growth advantage to at least one azole. Of those, 1,117 are resistant to multiple azoles, with 64% (712) being resistant to all of the azoles tested (Fig. 5a). Cross-resistance, whereby a mutation is advantageous in more than one azole, is therefore very common for this class of antifungal. Additionally, one third of the cross-resistance mutations (252/712) are attainable through only one nucleotide change from the wild-type *C. albicans* sequence. This implies that an organism can very quickly become resistant to all azoles.

To further rationalize the resistance conferred by certain amino acid substitutions, we examined whether the alteration in amino acid properties was significantly different between the categories of variants. Notably, a dissimilarity in amino acid properties was observed between resistant and neutral variants (chi-squared test, $P = 0.0003$), but not with deleterious variants (chi-squared test, $P = 0.97$) (Fig. 5a). Consequently, the general shift in amino acid properties alone cannot account for the observed resistance.

We note some interesting exceptions to cross-resistance. We categorized 151 variants to be resistant to only one azole. For instance, almost all variants at position 505 confer resistance to fluconazole and voriconazole, some to itraconazole, posaconazole and isavuconazole and none to clotrimazole. Similarly, more variants at position 464 are resistant to fluconazole and voriconazole in comparison to other azoles. Interestingly, G464S is one of the most often reported resistance mutations in the literature[12,42], and it is the only variant at position 464 resistant to all azoles in our experiment. Upon individual validation of variants, we identified five variants with an increased growth compared to the wild-type for a single azole. Subsequent validations conducted to ascertain the azole specificity of these variants revealed that 80% (4/5) displayed significantly higher growth than the wild-type in only one condition (Mann–Whitney U

test, $P < 0.05$) (Fig. 5b). Therefore, despite the drug-specific variants constituting a small proportion of the resistant variants, their presence is noteworthy and may yield valuable insights for targeted intervention strategies.

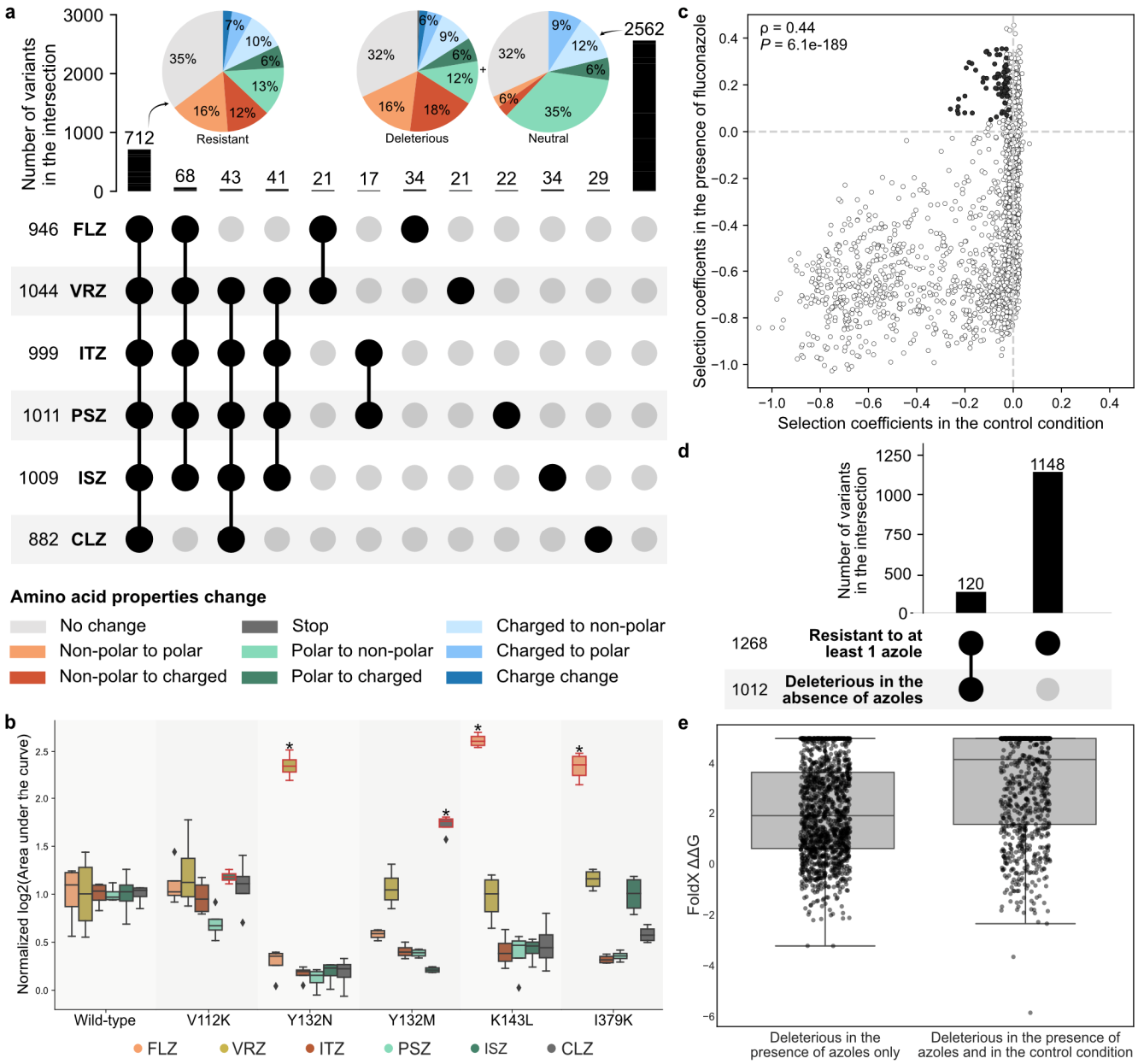

Fig. 5 | Azole resistance mutations in CaErg11 confer cross-resistance and rarely carry a fitness cost. a, Upset plot showing the intersection of azole resistant variants (black circles). The number of resistant variants for each azole is shown as well as the number of variants in the intersections. Only intersections with more than 15 variants are shown for clarity. Pie charts represent the change in amino acid properties for the intersection including variants resistant to all azoles and the intersection including variants neutral or deleterious for all azoles. FLZ: fluconazole, VRZ: voriconazole, ITZ: itraconazole, PSZ: posaconazole, ISZ: isavuconazole and CLZ: clotrimazole. **b,** Log2 of the area under the curve normalized relative to the wild-type for a subset of five variants that showed drug-specific resistance (n=4 replicates). These variants qualitatively had an increased growth compared to the wild-type only in the presence of one azole in the validations so we performed a second round of individual growth curves (red overlined boxplots: V112K: isavuconazole, Y132N: voriconazole, Y132M:

clotrimazole, K143L: fluconazole and I379K: fluconazole). 4/5 variants grew significantly more than the wild-type for only one azole, showing their specificity (*, Mann–Whitney U test, $P < 0.05$). Colors represent the different conditions and boxes represent the interquartile range. **c,** Selection coefficients of amino acid substitutions in fluconazole pooled competition assays compared with the control condition. Each value is the median of two synonymous codons per amino acid in most cases for the median of triplicate experimental measurements. The dark grey dots represent variants carrying a tradeoff, meaning that the mutation is advantageous in the presence of azole and significantly deleterious in the control condition. Spearman's rank correlation is shown. n = 3,830 amino acid variants. **d,** Upset plot showing the intersection of variants resistant to at least one azole and deleterious in the control condition. The number of variants for every group is shown as well as the number of variants in the intersections. **e,** Change in free energy (ΔΔG) predicted with FoldX for variants categorized as deleterious in the presence of antifungals. ΔΔG values are higher for variants deleterious in both the azole and control conditions (median ΔΔG of 4.16) compared to those deleterious only in azoles (median ΔΔG of 1.91) (Mann-Whitney U test, $P < 0.0001$). Values higher than five were rounded to five for plotting.

Most resistance mutations carry no significant fitness cost

As Erg11 is a key enzyme in the ergosterol biosynthesis pathway and since its canonical substrate sits in the same binding pocket as azoles, resistance mutations have a strong potential to carry a fitness cost in the absence of drugs. One would therefore expect a tradeoff between resistance and fitness in the absence of azoles. We first tested if there was a negative correlation between the selection coefficient of amino acid substitutions in azole and control conditions. A negative correlation would show that in general, resistance mutations negatively alter the enzyme function sufficiently to reduce growth in control conditions. Surprisingly, we only found positive correlations ($\rho = 0.43$ to 0.51, $P < 0.0001$) (Fig. 5c, Extended Data Fig. 13). This positive correlation shows that many mutations enhance drug resistance without altering protein function. Second, we examined the fraction of resistant variants that are also deleterious in the control condition. Our analysis revealed that only 9% (120) of resistant variants carry a significant fitness cost (Fig. 5e). Positions 140, 143 and 471 are particularly enriched for such tradeoffs, probably because of their interaction or proximity positions with the heme[47] (Fig. 3a). Since amino acid substitutions 143E and Q have been reported in clinical isolates[12,38], our results suggest that tradeoffs between resistance and fitness are relatively rare for Erg11 and that when they occur, they do not prevent mutations from occurring in clinical settings. Either selection is too strong for the tradeoffs to play a significant role or compensatory mutations or physiological mechanisms (e.g. upregulation or downregulation of other genes) reduce the impacts of costly mutations during drug treatment[19,53]. It is important to note that the experimental conditions used here do not necessarily reflect the selective pressure of the natural or clinical environments. Therefore, the proportion of tradeoff mutations could be more important if one considered other potential environments that could make the function of Erg11 even more critical or that could further enhance the impact of resistance amino acid substitutions, for instance elevated temperatures[17,54].

Even though few amino acid substitutions significantly impaired CaErg11 function in the control condition, a larger number were highly harmful in the presence of azoles (Fig. 2b-h) while having a mild or no effect in control conditions. Specifically, 26% (1,012 variants) were found

364 to be deleterious in the control condition (Fig. 5e), while this percentage increased to 58%
365 (2,204 variants) in azoles. It is likely that certain mutations slightly diminish the canonical
366 enzymatic reaction, without exerting a substantial impact on fitness under normal conditions.
367 However, their effects would be amplified in the presence of drugs that diminish the enzyme
368 function. We observed that the changes in free energy (ΔΔG) predicted with FoldX[49] are higher
369 for variants deleterious in both the azole and control conditions (median ΔΔG of 4.16) compared
370 to those deleterious only in azoles (median ΔΔG of 1.91) (Fig. 5e, Mann-Whitney U test, $P <$
371 0.0001). This is consistent with a slight destabilization by the mutations that reduce enzyme
372 activity but that is visible only when the drug further inhibits its function. Highly destabilizing
373 mutations on the other hand would already have an effect without azoles. Other drugs that
374 could destabilize Erg11 or reduce its abundance could therefore be interesting leads for
375 sensitizing fungi to azoles.

Discussion

376 Infections caused by fungal pathogens are a serious public health problem[55]. The emergence
377 of fungi resistant to antifungals threatens our ability to treat infections[10,11,56]. *C. albicans* is the
378 most frequent cause of fungal infections in humans, which are routinely treated with azole drugs
379 that inhibit the enzyme cytochrome P450 lanosterol 14-alpha-demethylase (Erg11). Despite the
380 key importance of this species and of Erg11 in clinical microbiology, our picture of the drug
381 resistance mechanisms conferred by mutations in *ERG11* is incomplete. Here, using a deep
382 mutational scanning approach, we created a library of nearly 4,000 variants of *C. albicans*
383 Erg11. The library was used to characterize resistance mutations to six medical azoles, leading
384 to more than 25,000 genotype-phenotype associations. For each drug, an average of 1,000
385 variants were found to confer resistance, which led to nearly 6,000 experimentally validated
386 drug-resistance associations. More than 50% of the resistant variants are resistant to all of the
387 azoles tested and less than 9% of them lead to a fitness defect in the absence of drugs. The
388 creation of an extensive catalog of Ca*ERG11* mutations leading to azole resistance will improve
389 genotype interpretation and could help treatment choice in clinical settings. In addition, the
390 systematic characterization of Ca*ERG11* variants allowed a better understanding of cross-
391 resistance and tradeoff which we hope will impact regulations linked to azole usage and help
392 develop new drugs. Using a similar approach on orthologs and on other fungal pathogen genes
393 could help fight fungal infection, and even give us a step ahead by identifying resistance
394 mutations before their spread in patients, in clinics and agriculture.

395 Although our experiments were performed on the *C. albicans* gene, the conservation of the
396 protein among orthologs may allow us to interpret the impact of mutations in other species. For
397 instance, mutation F444L was recently identified and validated as contributing to fluconazole
398 and voriconazole resistance in *C. auris*[57]. Here, we find that the homologous change F449L in
399 *C. albicans* also confers resistance ($s = 0.18$ and 0.22, $P < 0.0001$). In addition, Williamson *et*
400 *al.*[58] tested the susceptibility of five *C. auris* variants V125A, F126L, Y132F, K143R and I466M
401 (I471M in CaErg11) to fluconazole, voriconazole, itraconazole and posaconazole. We find

similar resistance phenotypes for I471M and K143R (s = 0.11 to 0.43, $P < 0.0001$) but not for the other mutations. For instance, they found that V125A conferred a 2-fold decrease in susceptibility to voriconazole and itraconazole, but not to fluconazole and posaconazole while we classified this variant as resistant to all of the azoles we examined (s = 0.13 to 0.26, $P < 0.0001$). It is possible that standard methods used by the authors to quantify susceptibility are not sensitive enough to detect small variations, thereby explaining the observed differences. In the more distantly related mold *A. fumigatus,* G54E, V, R and W substitutions confer resistance to itraconazole and posaconazole while maintaining susceptibility to voriconazole[33]. The residue at position 54, orthologous to G65 in *C. albicans,* is located in the substrate entry channel. In accordance with Sagatova *et al.* [59] who reproduced the mutations at the homologous position in *S. cerevisiae*, we did not detect an increase in azole resistance. We instead observed that two variants at position 54 have their growth impaired in the control conditions and that all variants are deleterious in azoles. The substitution from glycine to larger amino acids could restrict entry channel access for drug and substrate. The disparities of phenotypes may arise due to differences in protein structure, with *Aspergillus* being a more distant species. Some slight changes could have occurred either on the branch leading to *Aspergillus* or the one leading to the yeast clade. Nonetheless, some resistance phenotypes are consistent between *C. albicans* and *A. fumigatus* mutations. For instance, *A. fumigatus* G138C and Y431C confer an approximately 10-fold increase in resistance to voriconazole, itraconazole and posaconazole[32]. Here, we also found that the homologous substitutions A149C and Y447C confer resistance to all of the azoles tested (s = 0.19 to 0.28, $P < 0.0001$). To help the community to perform such comparisons, we provide the selection coefficients and corresponding categories obtained for each CaErg11 variant at orthologous positions in fungal pathogens as a resource (Supplementary data 4).

In the future, it will be important to further investigate the different determinants of azole resistance mutations between *ERG11* orthologues and all azole drugs. For instance, azoles are also used in agriculture and evidence shows that azole-resistant *A. fumigatus* from the environment can infect patients leading to an increase in treatment failures[14,16,60]. This is alarming as it implies the presence of cross-resistance between agricultural and medical azoles[15,61,62]. The azoles used in agriculture are not the same as the ones used in clinics, but they have chemical similarities and they share the same mechanism of action. Given the extent of cross-resistance and the very limited tradeoff we measured here, the selective forces that represent the use of azoles in contexts such as in agriculture should be considered as a serious threat to the longevity of azoles for successfully treating some fungal infections[63,64].

Acknowledgement

We thank the members of the Landry lab for supportive advice and discussion on the project and Philippe Després and Romain Durand for sharing some bioinformatics material for data analysis. We also thank Aleeza Gerstein, Rong Shi and Sophie Gobeil for their advice and comments throughout the project.

Author contributions

CRL, CB, IGA, LM and RSS designed research. CB, IGA, JB, SP, AKD, JS performed experiments. AP and CB generated in silico data. CB analyzed data. CB produced figures. CB and CRL drafted the manuscript. All authors contributed to editing the manuscript.

Financial support

This project was funded by a Canadian Institutes of Health Research (CIHR) Foundation grant number 387697 to CRL, a Fonds de recherche du Québec Nature et technologies (FRQNT) Team Grant (2022-PR-298169), a Genome Canada and Genome Quebec grant (6569 to CRL) and a Natural Sciences and Engineering Research Council of Canada (NSERC) Discovery Grant (RGPIN-2018-4914) to RSS. CRL holds the Canada Research Chair (Tier I) in Cellular Systems and Synthetic Biology. RSS holds the Canada Research Chair (Tier II) in Microbial Functional Genomics. CB was supported by fellowships from FRQNT, Fonds de Recherche du Québec Santé (FRQS), NSERC, EvoFunPath NSERC Collaborative Research and Training Experience (CREATE) program and Université Laval. JB was supported by fellowships from NSERC and FRQNT. LM was supported by a fellowship from the EvoFunPath NSERC CREATE program.

Data availability

Raw sequencing reads from pooled competitions are available at BioProject PRJNA1044755. Read counts for DNA variants are available in Supplementary data 5, sample descriptions in Supplementary data 6 and overall read counts through quality control for every sample in Supplementary data 7. All scripts for figures and analysis are available on GitHub at https://github.com/Landrylab/Bedard_et_al_2023 with their input and output files.

Methods

Strains, antimicrobials and culture media

459 *Escherichia coli* MC1061 ([*araD139*]$_{B/r}$ Δ(*araA-leu*)*7697* Δ*lacX74 galK16 galE15(GalS) λ-e14-*
460 *mcrA0 relA1 rpsL150(strR) spoT1 mcrB1 hsdR2*) was used for all cloning steps. *S. cerevisiae*
461 R1158[65] (*URA3*::CMV-tTA *MAT**a** his3-1 leu2-0 met15-0*) was the background strain used to
462 construct *ScERG11*-DOX strain (Yeast strain construction section). *C. albicans* SC5314[66] was
463 the background strain used for genome editing and physiological profiling.

464 Nourseothricin (NAT, Cedarlane Labs : AB-102-25G), doxycycline (DOX, BioShop :
465 DOX444.1), geneticin (G418, BioShop : GEN418.10) and ampicillin (AMP, BioShop :
466 AMP201.25) were solubilized in water at a 1000X stock concentration, filtered and frozen at -
467 20 °C. Fluconazole (Cedarlane Labs : 11594-500), voriconazole (TCI America : V0116),
468 itraconazole (Sigma-Aldrich : I6657), posaconazole (Sigma-Aldrich : 32103), isavuconazole
469 (Sigma-Aldrich : SML2357), clotrimazole (TCI America : C28675G) were solubilized in dimethyl
470 sulfoxide (DMSO) at 1000X stock concentration and stored at -20 °C.

471 For liquid cultures, bacteria were grown in LB medium (0.5% yeast extract, 1% tryptone and
472 1% sodium chloride) at 37 °C in a shaking incubator (250 rpm). For solid culture, bacteria were
473 grown on 2YT medium with glucose and 2% agar (1% yeast extract, 1.6% tryptone, 0.5%
474 sodium chloride and 0.2% glucose) and incubated at 37 °C. For bacterial transformations,
475 medium was supplemented with 100 µg/mL AMP. Yeast were grown in YPD medium (1% yeast
476 extract, 2% tryptone and 2% glucose) at 30 °C in a shaking incubator (250 rpm). On solid
477 medium, 2% agar was added to YPD and yeasts were grown at 30 °C. Yeast transformants
478 with pRS31N plasmids were selected on YPD medium supplemented with 100 µg/mL of NAT.

Plasmids construction

479 All PCRs in this section were done using the KAPA HiFi HotStart polymerase (Roche :
480 07958897001). For all PCR amplification products used for cloning, 20 U of DpnI (New England
481 Biolabs : R0176S) was added to the PCR products and incubated at 37 °C for 1 hour to remove
482 the parental PCR DNA template. The digested amplicons were purified on magnetic beads
483 (Axygen AxyPrep Mag PCR Clean-Up Kit). The vectors and inserts were assembled following
484 the Gibson DNA assembly protocol[67]. Oligos and plasmids are listed in Supplementary data 8.

485 *Candida albicans ERG11* (*CaERG11*) was expressed from a yeast centromeric plasmid
486 pRS31N-*CaERG11* constructed as follows. First, we created a plasmid containing the *S.*
487 *cerevisiae ERG11* (*ScERG11*) sequence, including its promoter and terminator. We assembled
488 pRS31N-*ScERG11* as follows. The plasmid pRS31N[68] containing AMP and NAT resistance
489 markers was amplified using this PCR mix and cycles:

	Name	**Concentration**	**Volume (µL)**
DNA	pRS31N	10 ng/µL	1.00
Buffer	Fidelity buffer	5X	5.00
dNTPs		10 mM	0.75
Oligo F	OP252-A10	10 µM	0.75
Oligo R	OP252-B10	10 µM	0.75
Enzyme	KAPA	1 U/µL	0.30
Water			16.45
		Total volume	25.00

Time	**Temperature**	**Number of cycles**
5 min	95°C	1x
20 sec	98°C	35x
15 sec	66°C	
3 min	72°C	
3 min	72°C	1x
Hold	10°C	

490 The *S. cerevisiae ERG11* native promoter (878 base pairs), coding sequence (1593 base pairs)
491 and terminator (319 base pairs) were amplified from the pMoBY-*ERG11* plasmid[69] with primers
492 adding homology to the pRS31N plasmid cloning site:

	Name	**Concentration**	**Volume (µL)**
DNA	pMoBY-*ERG11*	10 ng/µL	1.00
Buffer	Fidelity buffer	5X	5.00
dNTPs		10 mM	0.75
Oligo F	OP252-C10	10 µM	0.75
Oligo R	OP252-D10	10 µM	0.75
Enzyme	KAPA	1 U/µL	0.30
Water			16.45
		Total volume	25.00

Time	Temperature	Number of cycles
5 min	95°C	1x
20 sec	98°C	5x
15 sec	61°C	
2 min	72°C	
20 sec	98°C	30x
15 sec	68°C	
2 min	72°C	
3 min	72°C	1x
Hold	10°C	

The vector and the insert were assembled to obtain pRS31N-*ScERG11*.

For the second step to construct pRS31N-*CaERG11*, pRS31N-*ScERG11* was amplified to remove the *ScERG11* sequence and keep the native promoter and terminator:

	Name	Concentration	Volume (µL)
DNA	pRS31N-*ScERG11*	10 ng/µL	1.00
Buffer	Fidelity buffer	5X	5.00
dNTPs		10 mM	0.75
Oligo F	OP252-G8	10 µM	0.75
Oligo R	OP252-H8	10 µM	0.75
Enzyme	KAPA	1 U/µL	0.30
Water			16.45
		Total volume	25.00

Time	Temperature	Number of cycles
5 min	95°C	1x
20 sec	98°C	35x
15 sec	63°C	
6 min	72°C	
8 min	72°C	1x
Hold	10°C	

To ensure the expression of *CaERG11* in *S. cerevisiae* (*C. albicans* decodes the CTG codon differently[70]), the *CaERG11* sequence (from SC5314 strain[66], Candida Genome Database (CGD): C5_00660C_A) was codon optimized for *S. cerevisiae* (GenScript). The sequence was synthetized by GenScript and amplified by adding homology to the *ScERG11* promoter and terminator, so it could replace the *ScERG11* coding sequence in pRS31N-*ScERG11*:

	Name	Concentration	Volume (µL)
DNA	pUC19-*CaERG11*	10 ng/µL	1.00
Buffer	Fidelity buffer	5X	5.00
dNTPs		10 mM	0.75
Oligo F	OP252-C8	10 µM	0.75
Oligo R	OP252-D8	10 µM	0.75
Enzyme	KAPA	1 U/µL	0.30
Water			16.45
		Total volume	25.00

Time	Temperature	Number of cycles
5 min	95°C	1x
20 sec	98°C	5x
15 sec	60°C	
1 min	72°C	
20 sec	98°C	30x
15 sec	68°C	
1 min	72°C	
2 min	72°C	1x
Hold	10°C	

501 The vector and the insert were cloned to obtain pRS31N-*CaERG11*.

502 The variant library (see below for library design and construction) was cloned in pRS31N-
503 Barcode, a plasmid containing a NdeI restriction site, a 20N barcode and universal priming sites
504 for subsequent amplifications. To construct this plasmid, pRS31N-*ScERG11* was amplified
505 without *ScERG11* and the terminator. The forward oligo added the priming sites and the
506 barcode:

	Name	Concentration	Volume (µL)
DNA	pRS31N-*ScERG11*	10 ng/µL	5.00
Buffer	Fidelity buffer	5X	5.00
dNTPs		10 mM	0.75
Oligo F	CLOP259-F3	10 µM	2.00
Oligo R	CLOP252-H8	10 µM	2.00
Enzyme	KAPA	1 U/µL	0.30
Water			9.95
		Total volume	25.00

Time	Temperature	Number of cycles
5 min	95°C	1x
20 sec	98°C	18x
15 sec	62°C	
5 min	72°C	
3 min	72°C	1x
Hold	10°C	

507 From pRS31N-*ScERG11*, the terminator was amplified with oligos adding a NdeI restriction site
508 and homology to the vector:

	Name	Concentration	Volume (µL)
DNA	pRS31N-*ScERG11*	10 ng/µL	1.00
Buffer	Fidelity buffer	5X	5.00
dNTPs		10 mM	0.75
Oligo F	CLOP259-D3	10 µM	0.75
Oligo R	CLOP259-E3	10 µM	0.75
Enzyme	KAPA	1 U/µL	0.30
Water			16.45
		Total volume	25.00

Time	Temperature	Number of cycles
5 min	95°C	1x
20 sec	98°C	5x
15 sec	64°C	
15 sec	72°C	
20 sec	98°C	30x
15 sec	70°C	
15 sec	72°C	
3 min	72°C	1x
Hold	10°C	

509 The vector and the insert were cloned to obtain pRS31N-Barcode. To preserve barcode
510 diversity, we added 5 mL of 2YT medium to the plates with colonies following Gibson DNA
511 assembly, scraped them with a glass rake and used 1.5 mL of this mix to extract plasmids.

Yeast strain construction

512 The construction of the *ERG11* repressible strain of *S. cerevisiae* (*ScERG11*-DOX) was based
513 on the Yeast Tet-Promoters Hughes collection (yTHC)[39]. The endogenous promoter of *ERG11*
514 (50 bp before the ATG codon of ERG11, chrVIII:121683..121733) was replaced with a TET-
515 titratable promoter repressible with doxycycline (DOX). The *ScERG11*-DOX strain was

516 constructed as follows. The *KANMX*-tetO$_7$ cassette (Hughes et al. 2000) was amplified from
517 pKB33[71]:

	Name	Concentration	Volume (µL)
DNA	pKB33	10 ng/µL	0.75
Buffer	Reaction buffer	5X	5.00
dNTPs		10 mM	0.50
Oligo F	CLOP258-G6	10 µM	1.25
Oligo R	CLOP258-D7	10 µM	1.25
Enzyme	Q5*	1 U/µL	0.25
Water			16.00
		Total volume	25.00

*Q5 High-Fidelity DNA Polymerase (NEB : M0491L)

Time	Temperature	Number of cycles
5 min	95°C	1x
20 sec	98°C	5x
15 sec	66°C	
2 min	72°C	
20 sec	98°C	30x
15 sec	70°C	
2 min	72°C	
3 min	72°C	1x
Hold	10°C	

518 Competent cells of *S. cerevisiae* R1158[65] were transformed with the amplified *KANMX*-tetO$_7$
519 cassette using a standard lithium acetate transformation protocol[72]. G418 was added to the
520 medium at a concentration of 200 µg/mL. The resulting *ScERG11*-DOX strain has the genotype
521 pERG11::kanR-tetO$_7$-TATA *URA3*::CMV-tTA *MAT**a** his3-1 leu2-0 met15-0*.

Dose-response curves

522 Yeasts were grown in 96-well plates containing 200 µL of YPD medium with NAT, DOX and
523 azole at a starting optical density at 600 nm (OD_{600}) of 0.01. OD_{600} was measured in a Tecan
524 Infinite M Nano (Tecan Life Sciences) every 15 minutes for 24 hours without agitation and at
525 30 °C. The maximum growth rates were calculated from growth curves across a minimum of
526 17 drug concentrations, in triplicate for fluconazole and in duplicate for other azoles. The
527 maximum growth rates were transformed into relative inhibition to get dose-response curves.
528 Hill equation was fitted to the dose-response curves to determine the minimal inhibitory
529 concentration at 50% (IC_{50}). The analysis was based on Durand *et al*[73].

Library design

530 The selection of positions to mutate to create the CaErg11 deep mutational scanning library
531 was done using the ScErg11 structures. The crystal structures of ScErg11 bound to lanosterol
532 (4LXJ), fluconazole (4WMZ) and itraconazole (5EQB) were taken from the Protein Data Bank
533 (PDB) and used to calculate the distances between the residues and the substrates and the
534 heme molecule. The distances were compared with residues with known or putative resistance
535 mutations from the MARDy database[74]. A radius of 12 Å covering the active site and most
536 residues with known resistance mutations was selected. An alignment between ScErg11 and
537 CaErg11 using the Biopython toolkit (pairwise, global, BLOSUM62)[75] was used to select the
538 homologous residues in the *C. albicans* ortholog with a custom script. ScErg11 and CaErg11
539 sequences have a sequence identity of 62.7%. Consequently, their 3D structures are very
540 similar (Extended Data Fig. 2). The identity between ScErg11 and CaErg11 for the 206 residues
541 in the 12 Å radius is 85.9%. The selected residues are listed in the Supplementary data 1.

542 In the CaErg11 variant library, each of the 206 targeted residues were replaced by the 19 non-
543 wild type amino acids encoded by two codons, when possible (methionine and tryptophan are
544 encoded by only one codon, Supplementary data 2). For each amino acid, we selected the two
545 most frequently used codons in the *ScERG11* ortholog to minimize the potential impact of
546 codon usage on expression. As controls, a stop codon was introduced at every 20 positions
547 along the sequence. A total of 7,839 DNA variants were designed. We ordered the synthesized
548 DNA variants from Twist Bioscience (QC report, Supplementary data 9). Positions 92, 228, 232,
549 233 and 234 failed to be synthesized, so they are missing from the library. The library used
550 covers a total of 3,830 amino acid variants. The library was split into four fragments (F1, F2, F3
551 and F4) of around 400 base pairs with overlapping positions. Fragment 1 goes from residue 44
552 to 176, fragment 2 goes from residue 147 to 288, fragment 3 goes from residue 269 to 413 and
553 fragment 4 goes from residue 386 to 520.

554 **Library construction**

555 The variant sequences have a flanking region of 35 base pairs from the native *ScERG11*
556 promoter to clone into pRS31N-Barcode. To limit the risk of losing variant diversity, we clone
557 the variants position-by-position. The variant sequences were amplified with a reverse primer
558 adding homology to the *ScERG11* terminator using the following PCR mix and conditions:

	Name	Concentration	Volume (µL)
DNA	Twist DNA variants	1 ng/µL	1.00
Buffer	Fidelity buffer	5X	5.00
dNTPs		10 mM	0.75
Oligo F	CLOP259-D3	10 µM	0.75
Oligo R	CLOP259-E3	10 µM	0.75
Enzyme	KAPA	1 U/µL	0.30
Water			16.45
		Total volume	25.00

Time	Temperature	Number of cycles
5 min	95°C	1x
20 sec	98°C	5x
15 sec	60°C	
1 min	72°C	
20 sec	98°C	13x
15 sec	68°C	
1 min	72°C	
2 min	72°C	1x
Hold	10°C	

pRS31N-Barcode was digested with NdeI (NEB : R0111S) for 2 hours at 37°C and inactivated for 20 minutes at 65°C:

Component	Concentration	Volume (µL)
pRS31N-Barcode	93.1 ng/µL	21.5
CutSmart™ Buffer	10X	4.0
NdeI	20 U/µL	2.0
Water		12.5
		40.0

Variant sequences were cloned into the NdeI digested pRS31N-barcode plasmid by Gibson DNA assembly[67]. We added 5 mL of 2YT medium to the plates , they were scraped with a glass rake and 1.5 mL was used to extract plasmids for yeast transformations.

The plasmid variant library was transformed position-by-position in competent *ScERG11*-DOX yeast cells using a standard lithium acetate transformation protocol[72]. We added 5 mL of YPD medium to the plates and scraped with a glass rake. All CaErg11 library positions were finally pooled by fragment in equivalent of OD_{600} units and archived in 25% glycerol at -80°C (Extended Data Fig. 3).

Library quality control

569 The yeast library was grown by pooling fragments and growing in liquid YPD+NAT medium
570 overnight. We aliquoted 5 OD_{600} units of cells into 1.5 mL microtubes and spun down at 600 x
571 g for 2 minutes. Then, after supernatant removal, 1 mL of YPD was added to resuspend the
572 pellets and cells were spun down again at 600 x g for 2 minutes. The supernatant was removed
573 by aspiration and the resulting pellets were kept at -80°C.

574 Plasmids were retrieved from yeast using the Zymoprep Yeast Plasmid Miniprep II kit (Zymo
575 Research : D2004). The protocol was modified according to Starr et al., 2020[76] and from our
576 own tests to increase yield. To frozen pellets, 200 µL of solution 1 was added. Then, 30 U of
577 Zymolyase™ (from the kit and from BioShop : ZYM002) was added. Cells were resuspended
578 by light vortexing and incubated at 37 °C for 2 hours. At the end of the incubation period, tubes
579 were lightly vortexed and frozen for at least 20 minutes at -80°C, and up to overnight. Frozen
580 tubes were thawed at 37°C for 3 minutes. After, 200 µL of solution 2 was added and mixed.
581 Then, 400 µL of solution 3 was added, mixed and tubes were centrifuged at maximum speed
582 for 3 minutes. The supernatant was transferred to the Zymo-Spin-I column (around 800 µL) and
583 spun for 30 seconds at maximum speed. To the column in a collection tube, 550 µL of wash
584 buffer with ethanol was added. Column was centrifuged for 1 minute 30 seconds at maximum
585 speed. The column was then placed into a new 1.5 mL microfuge tube, 10 µL of Tris 10 mM
586 pH 8 was added, and the tube was spun for 1 minute at maximum speed. The resulting elution
587 was conserved at -20°C.

588 Starting with 2 µL of yeast miniprep, *CaERG11* was amplified with a different primer pair for
589 each of the four fragments (F1: CLOP279-A6 + CLOP279-B8, F2: CLOP279-C6 + CLOP279-
590 D8, F3: CLOP279-E6 + CLOP279-F8, F4: CLOP279-G6 + CLOP279-H8) and annealing
591 temperature (**A** = F1: 61°C, F2 :60°C, F3: 58°C, F4: 62°C):

	Name	Concentration	Volume (µL)
DNA	Yeast miniprep	1 ng/µL	2.00
Buffer	Q5 buffer	5X	4.00
dNTPs		10 mM	0.40
Oligo F	CLOP279-F	2 µM	1.00
Oligo R	CLOP279-R	2 µM	1.00
Enzyme	Q5 (NEB)	1 U/µL	0.20
Water			11.40
		Total volume	20.00

Time	Temperature	Number of cycles
30 sec	98°C	1x
10 sec	98°C	23x
15 sec	**A**	
15 sec	72°C	
2 min	72°C	1x
Hold	10°C	

The amplicons were diluted 1:2,500 and used as a template for a second PCR adding Illumina sequencing adaptors. The reverse primer was unique for each fragment (F1: CLOP225-A1, F2: CLOP225-B1, F3: CLOP225-C1, F4: CLOP225-D1):

	Name	Concentration	Volume (µL)
DNA	*CaERG11* fragments	1/2500	1.00
Buffer	Fidelity buffer	5X	4.00
dNTPs		10 mM	0.60
Oligo F	CLOP224-A1	2 µM	3.00
Oligo R	CLOP225-R	2 µM	3.00
Enzyme	Kapa	1 U/µL	0.13
Water			8.27
		Total volume	20.00

Time	Temperature	Number of cycles
3 min	98°C	1x
30 sec	98°C	18x
15 sec	61°C	
35 sec	72°C	
1 min	72°C	1x
Hold	10°C	

599 Amplicons were purified on magnetic beads (Axygen AxyPrep Mag PCR Clean-Up Kit).

600 High-throughput sequencing was performed at the Centre de recherche du CHU de Québec -
601 Université Laval sequencing platform (CHUL, Québec) on an Illumina NovaSeq 6000 in 2x250
602 bp paired-end reads. The library was sequenced at roughly 100 reads per variant (F1: 7 million,
603 F2: 3 million, F3: 5 million, F4: 5 million) to estimate diversity and confirm the presence of every
604 variant. All mutations were confirmed to be present in the library, but a handful appeared to be
605 present at very low copy number (109CAG: 24 reads, 374ACT: 66 reads, 374CAA: 46 reads,
606 374GTC: 51 reads and 472TGT: 86 reads).

Pooled competition assay and high-throughput sequencing

607 We competed the *CaERG11* variants with and without azoles in a medium containing
608 doxycycline (10 µg/mL) to repress the endogenous copy of Sc*ERG11* and NAT (100 µg/mL)
609 for plasmid maintenance. Since antifungals were solubilized in DMSO, the control condition
610 also contained 0.1% DMSO. Azoles were used at concentrations inhibiting around 50% of the
611 wild-type growth (Extended Data Fig. 5) (fluconazole: 10.5 µg/mL, voriconazole: 0.12 µg/mL,
612 itraconazole: 0.10 µg/mL, posaconazole: 0.10 µg/mL, isavuconazole: 0.10 µg/mL and
613 clotrimazole: 0.30 µg/mL). We had to use lower concentrations for itraconazole and
614 isavuconazole than anticipated by our IC_{50} calculations as growth did not resume in these
615 conditions upon dilutions in the second round of competition.

616 Each of the four pools of the library were grown overnight in YPD+NAT starting with around
617 16,000 cells per variant and 2% of wild-type sequence (Timepoint 0, TP0). The saturated
618 cultures were transferred to fresh YPD+NAT+DOX+azole at a starting OD_{600} of 0.05 and grew
619 until an OD_{600} of 0.80 was reached (Timepoint 1, TP1). We did another transfer in fresh
620 YPD+NAT+DOX+azole at starting OD_{600} of 0.05, and let them grow until they reached an OD_{600}
621 of 0.80 (Timepoint 2, TP2) to achieve eight generations of competition (Extended Data Fig. 4).
622 At the end of every timepoint, 5 OD_{600} units of cells were aliquoted into tubes and spun down
623 at 600 x g for 2 minutes. Then, 1 mL of YPD was added to resuspend the pellets and spun
624 down again at 600 x g for 2 minutes. The resulting pellets were kept at -80 °C until they were
625 processed for plasmid extraction and sequencing. For the no antifungal condition, the same
626 protocol was used, but with 0.1% DMSO, and we added a third timepoint for a total of 12
627 generations.

Aliquoted pools of TP0 were prepared using the same protocol as in the "Library quality control" section. For TP2 (TP3 for the control condition), we aliquoted 5 OD_{600} of cells in 15 mL tubes and centrifuged at 916 x g for 5 min. Then, after supernatant removal, 1 mL of YPD was added to resuspend the pellets. The resuspensions were transferred in a 1.5 mL microtube and cells were spun down again at 600 x g for 2 min. The supernatant was removed by aspiration and the resulting pellets were kept at -80°C. Yeast minipreps and sequencing were done using the same protocol as in the "Library quality control" section. We used the primers listed in the sample files (Supplementary data 6) and sequenced at roughly 100 reads per variant (5 million reads per fragment, except for the control condition and in FLZ, F1= 7 million and F2= 3 million).

High-throughput sequencing analysis and variants count

High-throughput sequencing results were analyzed using custom scripts based on Després *et al.*[21] Each fragment has a different script but following the same steps. In the first part, quality control was done on demultiplexed reads with FastQC[77], reads were merged using PANDAseq[78] and trimmed according to oligos length and aggregated with VSEARCH[79]. Reads were then aligned to their corresponding *CaERG11* fragment using Needle from EMBOSS[80]. In the second part, Needle output files obtained were parsed to find mutations and count variants. As the library contains only single amino acid variants, we considered only reads where all the mutations detected were in the same codon when more than one mutation was detected.

Selection coefficient and characterization of the variants

The raw variant read counts were normalized by the total number of reads in their sequencing pool. The normalized read counts (N) of the initial timepoint (TP0) and the final timepoint (TP2) for the missense variants (mut) and the median normalized read counts for the variants with wild-type synonymous codons (med_WT) were used with the number of generations (G) to estimate a selection coefficient (*s*) of the variants using this equation[81]:

$$s = \frac{log_2\left(\frac{N_mut_TP2 \times N_med_WT_TP0}{N_mut_TP0 \times N_med_WT_TP2}\right)}{G}$$

We examined correlation between replicates (Extended data Fig.6), fragment overlaps (Extended data Fig.7) and synonymous codons (Extended data Fig.8) to measure the

654 reproducibility of the results. Only F4 of the fluconazole condition was not done at the same
655 moment as the others, hence it was not as linearly correlated with F3 as we saw for other
656 comparisons. This could have been caused by slight differences between batches of
657 experiments. To correct for this effect, we built an interpolation model to get new F4 values
658 following a linear regression with F3. The sequencing failed for 2 samples and they had to be
659 removed (Replicate A of F1 for voriconazole and Replicate C of F4 for itraconazole).

660 We classified the variants into three classes: beneficial, wild-type-like and deleterious. To do
661 so, we compared the variants with wild-type synonymous codons to missense variants with
662 two-sided independent *t-test* and corrected for multiple comparisons with the Benjamini-
663 Hochberg method. Variants with a false discovery rate (FDR) corrected *p-value* lower than 0.01
664 and with a positive selection coefficient were classified as beneficial, and those with a negative
665 selection coefficient, as deleterious. All variants with a p-value higher than 0.01 were classified
666 as neutral.

Validations by site-directed mutagenesis

667 The validation variants (Supplementary data 8) were constructed by site-directed mutagenesis
668 on the pRS31N-*CaERG11* plasmid. The mutagenesis primers designed were 40 base pair long
669 and identical to the sequence of the plasmid except for the bases we mutated:

	Name	**Concentration**	**Volume (µL)**
DNA	pRS31N-*CaERG11*	0.5 ng/µL	1.00
Buffer	Fidelity buffer	5X	5.00
dNTPs		10 mM	0.75
Oligo F	See Table XX	10 µM	0.75
Oligo R	See Table XX	10 µM	0.75
Enzyme	Kapa	1 U/µL	0.50
Water			16.25
		Total volume	25

Time	**Temperature**	**Number of cycles**
3 min	95°C	1x
20 sec	98°C	22x
15 sec	61°C	
10 min	72°C	
14 min	72°C	1x
Hold	10°C	

670 Every product of amplification was digested with 20 U of DpnI and incubated at 37°C for 1 hour.
671 Transformation in competent bacteria was done to retrieve the modified plasmids and the
672 mutations were confirmed by Sanger sequencing. Plasmids were transformed in competent
673 *ScERG11*-DOX cells using a standard lithium acetate transformation protocol[72].

674 Yeast were grown in YPD+DOX+NAT+0.1% DMSO and azoles as described in the dose-
675 response curves section. Azole concentrations corresponding to the IC_{50} were used. The area
676 under the curve (AUC) was extracted from the resulting growth curves using the composite
677 trapezoidal rule.

Candida albicans **genome editing**

678 We constructed pRS118, a plasmid derived from a previously described Candida-optimized
679 Cas9 plasmid (pRS252)[82,83]. An sgRNA cloning locus (containing sgRNA promoter, SNR52 and
680 the sgRNA tail) was cloned into pRS252 to generate pRS118. To create the H468T mutation in
681 the *ERG11* gene, CRISPR-Cas9 was first used to mediate a double-stranded break and then
682 the cells were supplied with the desired repair template. The sgRNA (oRS1335) for CaErg11 is
683 a 20 bp sequence that was designed using the sgRNA design tool Eukaryotic Pathogen
684 CRISPR gRNA Design Tool (EuPaGDT; http://grna.ctegd.uga.edu) which suggests guides
685 based on specificity and efficiency[84]. This sgRNA targeted 378 bp downstream of the *ERG11*
686 gene and was ordered from Integrated DNA Technologies (IDT). The sgRNA was then
687 duplexed and cloned in the *C. albicans*-specific CRISPR-Cas9 plasmid, pRS118, using SapI-
688 specific Golden Gate cloning, as described in Wensing *et al.*[85] to generate pRS684. The repair
689 template (gRS92) was ordered as a 971 bp gBlock gene fragment from IDT. This DNA fragment
690 contains the mutations (CAT468ACC) and the modified PAM sequence (AGG to CGA) that
691 prevents further cutting by pRS118's Cas9 upon successful insertion of gRS92.

692 The repair template was amplified by PCR using the following conditions:

	Name	Concentration	Volume (µL)
DNA	gRS92	50 ng/µL	0.2
Buffer	HF buffer	5X	4.0
dNTPs		10mM	0.4
Oligo F	oRS1340	100 µM	0.1
Oligo R	oRS1341	100 µM	0.1
Enzyme	Phusion*	2 U/µL	0.2
Water			10.0
		Total volume	15.0

*Phusion high-fidelity (HF) DNA polymerase (NEB : M0530S)

Time	Temperature	Number of cycles
5 min	98°C	1x
30 sec	98°C	35x
30 sec	61°C	
45 sec	72°C	
5 min	72°C	1x
Hold	4°C	

693 A lithium acetate transformation protocol was used to transform pRS684 into the SC5314
694 strain[85]. PacI-linearized plasmid and 100 µl of the amplified repair template was added to
695 SC5314 in the LiAc transformation mix, heat shocked and recovered on YPD medium plates
696 supplemented with 250 µg/mL of NAT[85]. Successful transformants with the plasmid inserted
697 into the *NEUT5L* locus were confirmed using PCR. Sanger sequencing was used to confirm
698 the *ERG11* heterozygous genotype for H468T.

699 We confirmed the resistance phenotype of the edited strain by spot assays. Cell density was
700 adjusted at 1 of OD_{600} and diluted 1/5 four times. We spotted 5 µL on YPD media (YPD +
701 DMSO, YPD + 2 µg/mL FLZ and YPD + 4 µg/mL FLZ) and incubated at 30°C for 24h.

In silico data and bioinformatic analysis

702 We ran GEMME[48] directly on the webserver (GEMME (upmc.fr)). As suggested in the
703 instructions, we generated the multiple sequence alignment using MMseqs2 via ColabFold
704 (A3M format)[86] with CaErg11 sequence (CGD : C5_00660C_A) and uploaded the A3M file. We
705 kept all default parameters (Number of iterations : 2 and Maximum number of sequences :
706 20,000). We used the data from the combined model (normPred_evolCombi.txt).

We used the MutateX package[87] to run an in silico mutation scan of CaErg11 with foldX 5[49,88]. We used CaErg11 structure bound to itraconazole (PDB ID : 5V5Z) for this analysis. Heme iron and itraconazole were parameterized with the pyFoldX paramx package[89] generating JSON files for those small molecules to be recognized by foldX. MutateX protocol runs RepairPDB, BuildModel and AnalyseComplexe commands from foldX to compute changes in protein free energy. The number of runs was set to 5. We analyzed interaction energy between the protein and antifungal drug as well as with the heme cofactor. Foldx ddG values higher than 5 were rounded to 5.

The visualization of protein structures was done with ChimeraX[90]. Figures and analysis were done using the following Python packages: Matplotlib[91], NumPy[92], UpSet[93], SciPy[94], pandas[95] and seaborn[96].

Supplementary figures

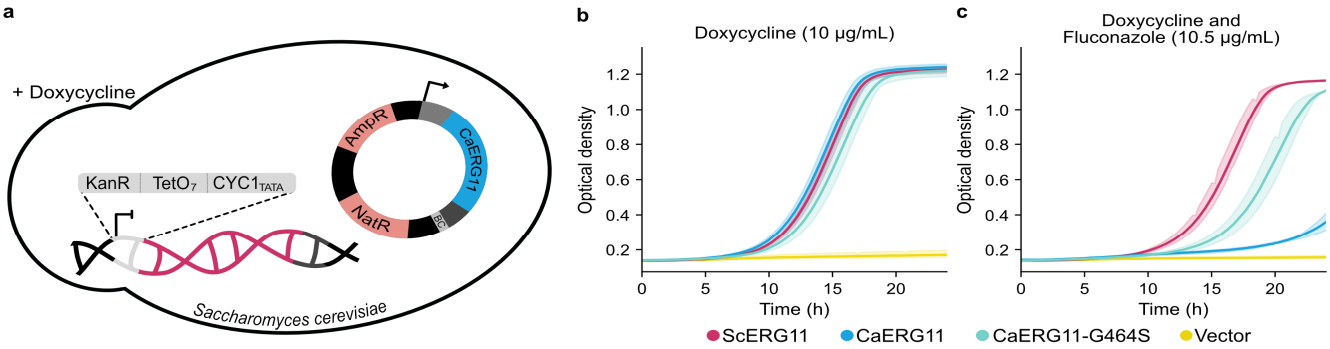

718 **Extended Data Fig. 1 | *ScERG11*-DOX strain repression and *CaERG11* complementation and resistance. a,**
719 The endogenous promoter of *ScERG11* was replaced with a doxycycline (DOX) repressible promoter that is fully
720 activated in the absence of DOX, but repressed in the presence of DOX (strain *ScERG11*-DOX[39]). *CaERG11* is
721 expressed from a plasmid containing the native promoter and terminator of *ScERG11*, *CaERG11*, a 20N barcode
722 (BC) and AmpR and NatR resistance markers. **b,c** OD_{600} was measured in YPD+NAT medium with DOX (10
723 µg/mL) to validate *ScERG11* repression in the *ScERG11*-DOX strain (**b**) and with DOX (10 µg/mL) and fluconazole
724 (10.5 µg/mL) to validate *CaERG11* complementation and resistance (**c**). When *ScERG11*-DOX is transformed
725 with an empty plasmid, there is no growth, as expected since *ERG11* is essential for *S. cerevisiae.* Growth is
726 restored when *ScERG11* is expressed from the plasmid. Transformation with the *CaERG11* plasmid rescues
727 growth, showing that *CaERG11* complements the function of *ScERG11*. *ScERG11*-DOX transformed with the
728 *CaERG11* plasmid is susceptible to fluconazole. When *ScERG11*-DOX is transformed with the plasmid expressing
729 *CaERG11*-G464S, a substitution known to confer fluconazole resistance[41], growth has recovered. The colored
730 bands represent standard deviations of the measurements, n=3.

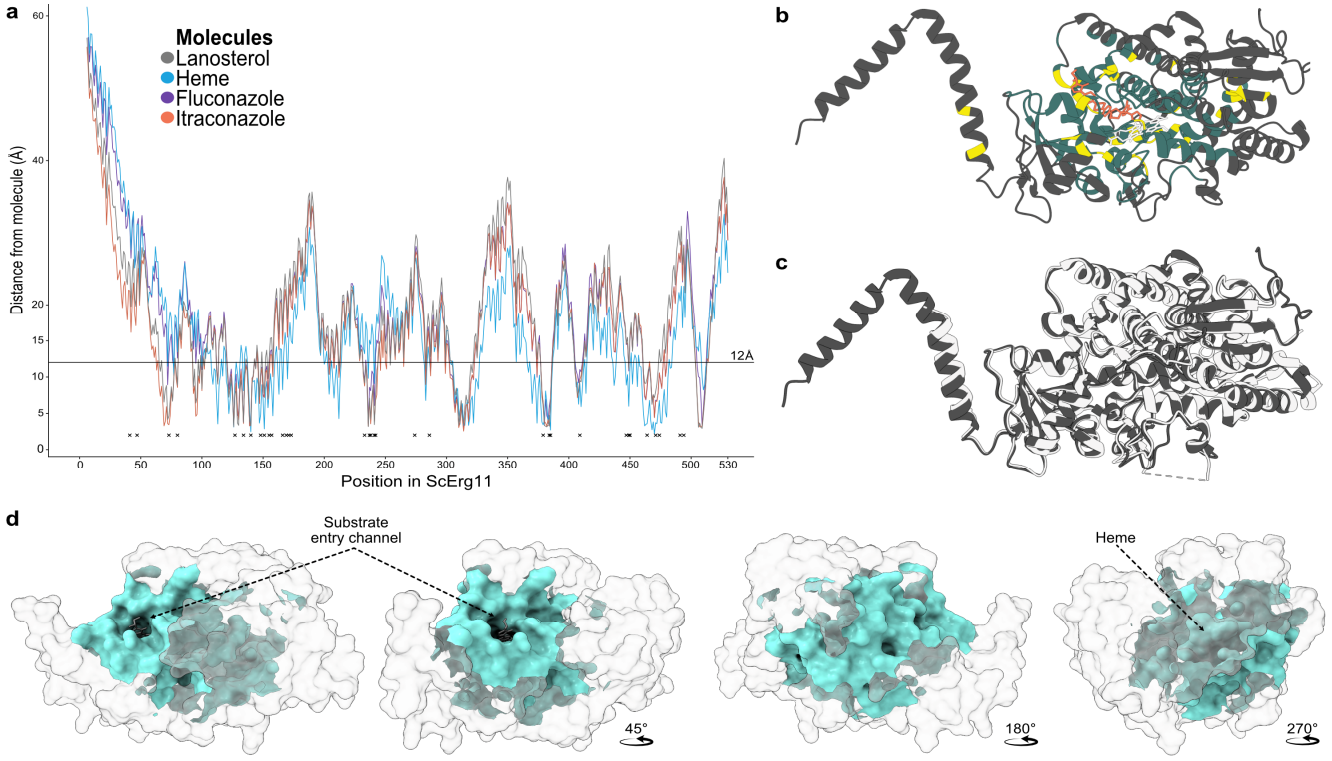

731 **Extended Data Fig. 2 | Selection of residues to be mutated in CaErg11 using the ScErg11 structures. a,**
732 Structures of ScErg11 bound to lanosterol (PDB ID: 4LXJ), fluconazole (PDB ID: 4WMZ) and itraconazole (PDB
733 ID: 5EQB) were used to calculate the distances in ångström (Å) between the molecules and amino acids.The Xs
734 represent positions with known resistance mutations listed in the MARDy database[74]. All residues at less than 12
735 Å from the lanosterol, the fluconazole, the itraconazole and the heme of ScErg11 were selected . **b,** We selected
736 a radius covering most residues (206, dark green) with known mutations in the MARDy database (yellow[74]), even
737 though most of them had not been validated. On the structure, ScErg11 is bound to itraconazole (orange) and an
738 heme (white) (PDB ID: 5EQB). **c,** ScErg11 (dark grey, PDB ID: 5EQB) superposed on CaErg11 (light grey, PDB
739 ID: 5V5Z). **d,** CaErg11 bound to itraconazole (PDB ID: 5V5Z). The 206 residues mutated in the variant library of
740 CaErg11 surround the ligand binding site (cyan).

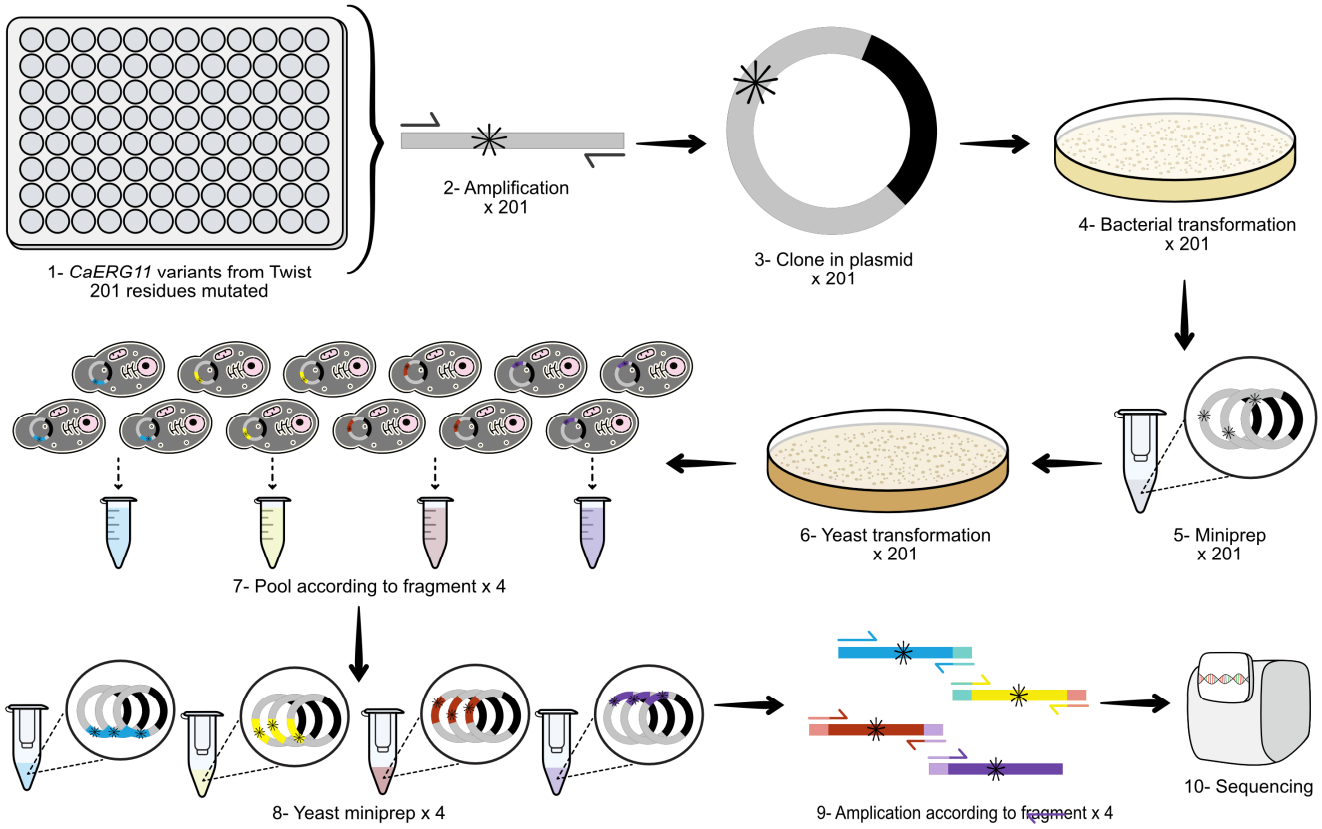

Extended Data Fig. 3 | Construction and validation of the *CaERG11* variant library. 1- *CaERG11* DNA variants were synthesized (Twist Bioscience). Each well of 96-well plates contained DNA fragments corresponding to one mutated position. 2- *CaERG11* DNA variants (*) were amplified and 3- cloned in a plasmid containing the native promoter and terminator of *S. cerevisiae ERG11* to ensure that expression regulation is representative of the native gene. 4- Plasmids were transformed into bacteria, all colonies on the plates were scraped and 5- minipreps were done to retrieve the plasmids. 6- All the plasmids were transformed into the yeast strain *ScERG11*-DOX and colonies were collected from plates. 7- The *CaERG11* library was separated into pools corresponding to four overlapping fragments for screening. 8- Plasmids were extracted using yeast minipreps. 9- *ERG11* variants were amplified from plasmid DNA according to their corresponding fragments. 10- Variant diversity was assessed by high-throughput sequencing.

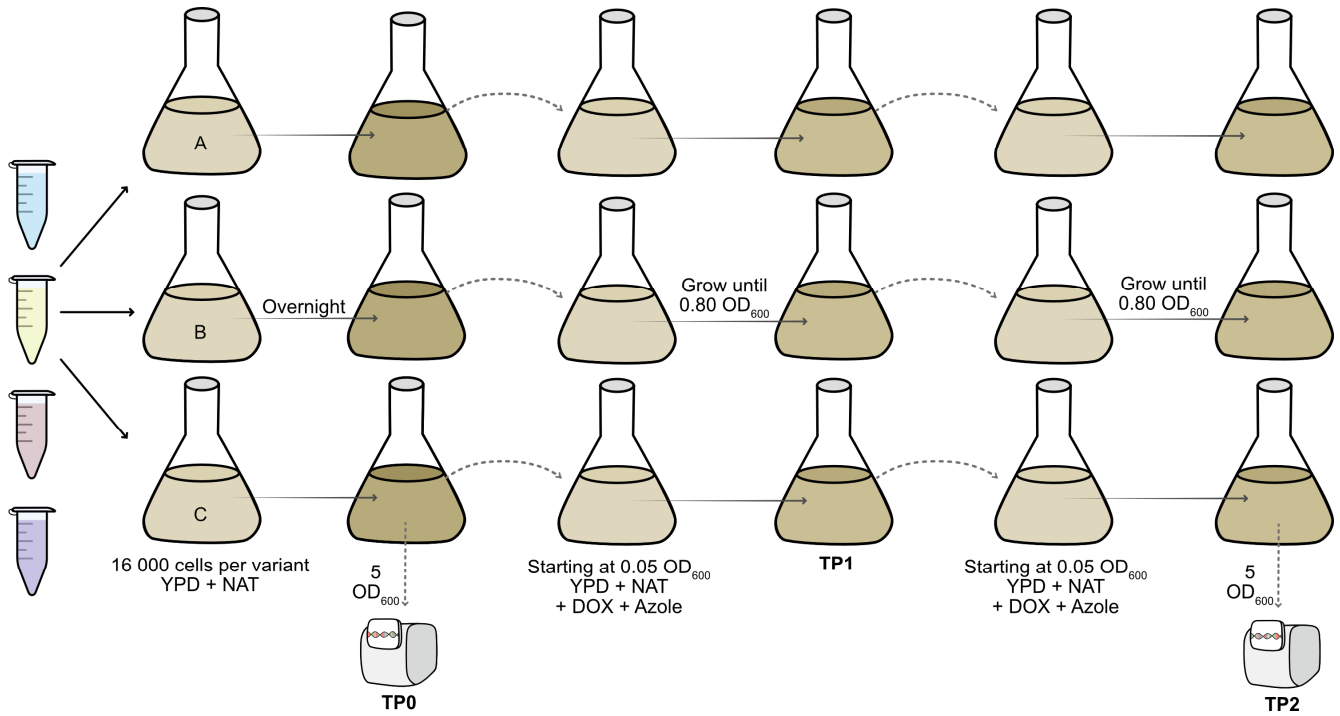

Extended Data Fig. 4 | Pooled competition assay of CaErg11 variants. All fragment pools were grown overnight in three replicates (A, B and C) in 25 mL of YPD+NAT medium starting with around 16,000 cells per variant (Timepoint 0, TP0). The saturated cultures were transferred to fresh YPD+NAT with doxycycline and azole at a starting OD_{600} of 0.05 and grown until an OD_{600} of 0.80 was reached (Timepoint 1, TP1). The cultures were transferred again into fresh YPD+NAT with doxycycline and azole at a starting OD_{600} of 0.05, and grown until they reached an OD_{600} 0.80 (Timepoint 2, TP2). The average number of generations per transfer was four, for a total of eight generations. At the end of TP0 and TP2, 5 OD_{600} units of cells were used for plasmid extraction and sequencing.

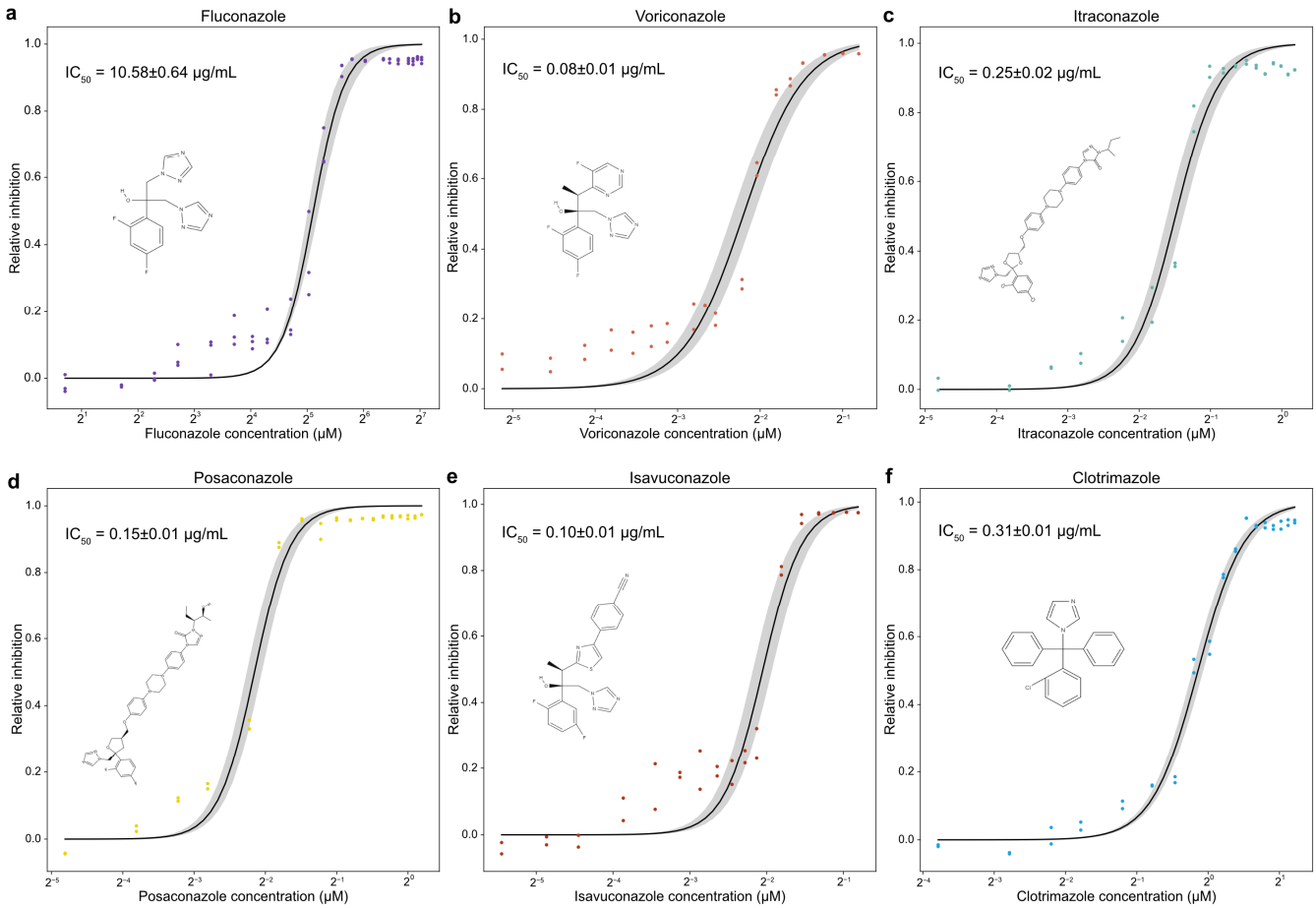

Extended Data Fig. 5 | Dose-response curves for the engineered strain *ScERG11*-DOX in the presence of six medical azoles. a,b,c,d,e,f, Relative growth inhibition as a function of drug concentration of fluconazole (**a**), voriconazole (**b**), itraconazole (**c**), posaconazole (**d**), isavuconazole (**e**) and clotrimazole (**f**). The growth of the *ScERG11*-DOX strain expressing *CaERG11* from a plasmid was measured in rich YPD+NAT medium containing doxycycline (10 μg/mL) . In each case, OD_{600} was measured every 15 minutes and the growth rates were estimated from the growth curves. Each point here represents a growth rate at a given drug concentration. The concentration corresponding to 50% inhibition (IC_{50}) is shown on the plots. Standard deviation is shown in light gray. Molecular structures were retrieved from PubChem[46]. n = 3 replicates for fluconazole and n = 2 for other drugs.

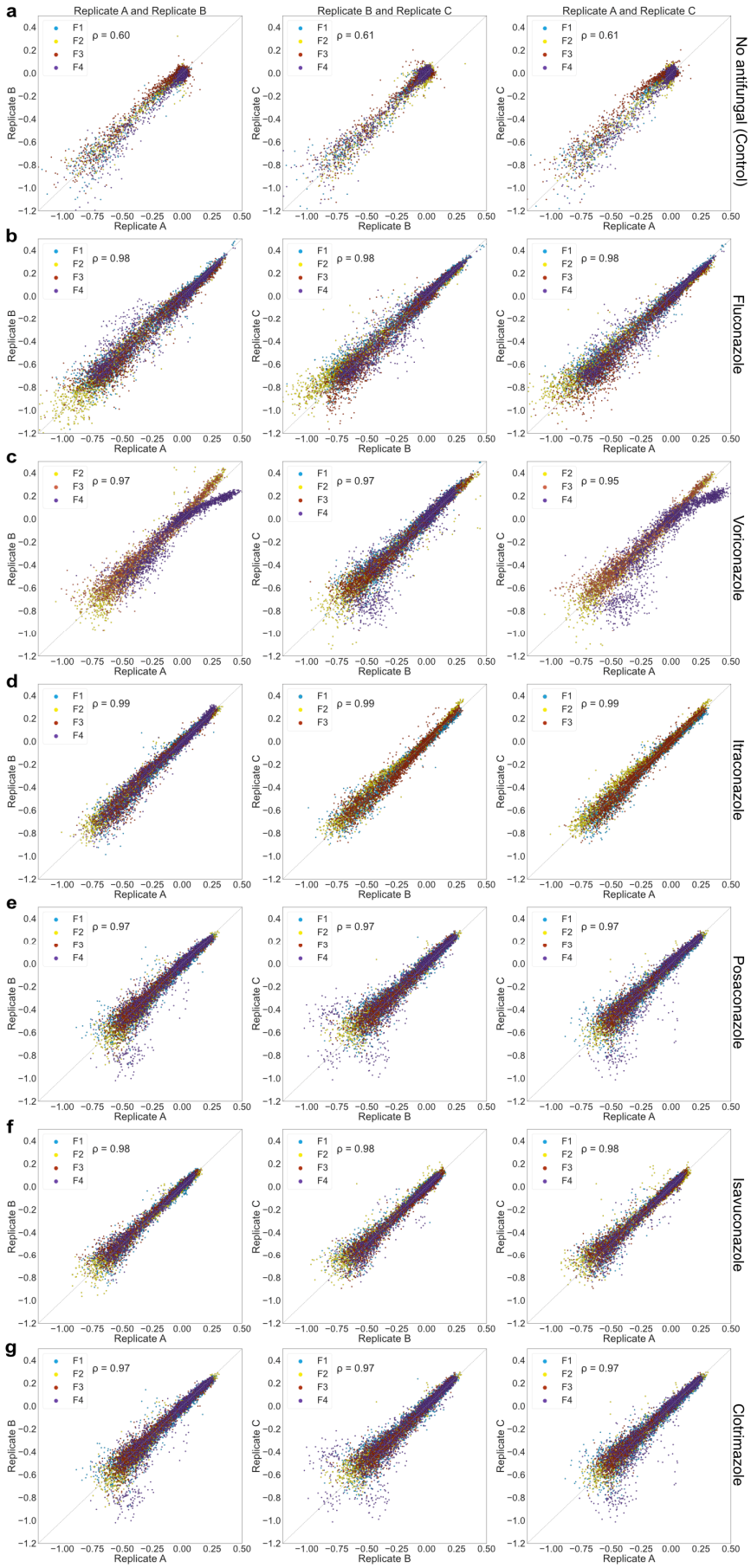
a
Replicate A and Replicate B
Replicate B and Replicate C
Replicate A and Replicate C
No antifungal (Control)
b
Fluconazole
c
Voriconazole
d
Itraconazole
e
Posaconazole
f
Isavuconazole
g
Clotrimazole
F1
F2
F3
F4
ρ = 0.60
ρ = 0.61
ρ = 0.61
ρ = 0.98
ρ = 0.98
ρ = 0.98
ρ = 0.97
ρ = 0.97
ρ = 0.95
ρ = 0.99
ρ = 0.99
ρ = 0.99
ρ = 0.97
ρ = 0.97
ρ = 0.97
ρ = 0.98
ρ = 0.98
ρ = 0.98
ρ = 0.97
ρ = 0.97
ρ = 0.97
Replicate A
Replicate B
Replicate C

767 **Extended Data Fig. 6 | Correlation between estimates of selection coefficients for individual codon variants**
768 **across replicated pooled competition assays. a,b,c,d,e,f,g,**. In control (**a**) and in fluconazole (**b**), voriconazole
769 (**c**), itraconazole (**d**), posaconazole (**e**), isavuconazole (**f**) and clotrimazole (**g**). Colors represent the four different
770 fragments. Replicate A of F1 for voriconazole and Replicate C of F4 for itraconazole had to be removed since
771 sequencing failed for these samples. Spearman's rank correlation is shown, $P < 0.0001$ in all cases. n = 7,649
772 DNA variants.

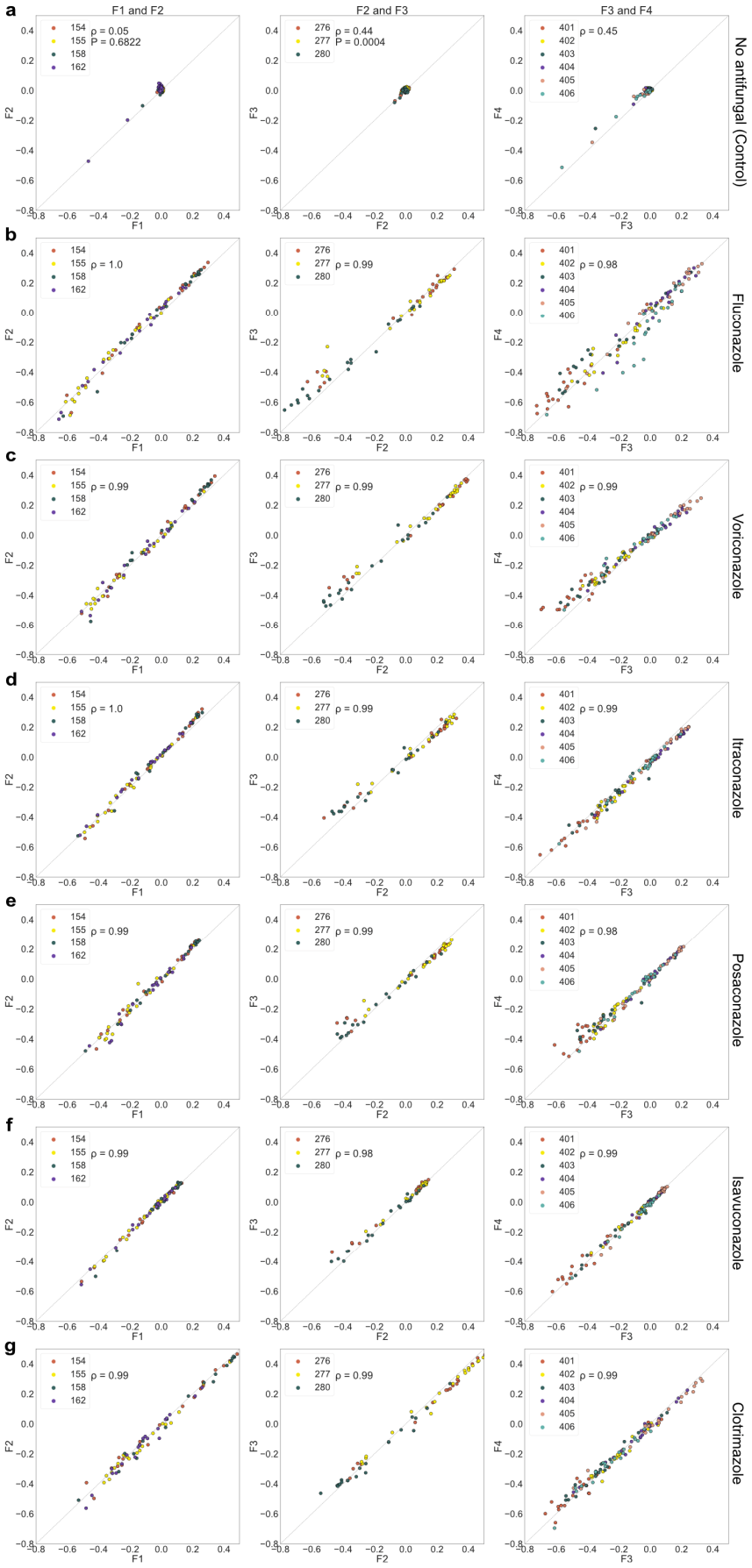
a
F1 and F2
F2 and F3
F3 and F4
154
155
158
162
ρ = 0.05
P = 0.6822
276
277
280
ρ = 0.44
P = 0.0004
401
402
403
404
405
406
ρ = 0.45
No antifungal (Control)
b
ρ = 1.0
ρ = 0.99
ρ = 0.98
Fluconazole
c
ρ = 0.99
ρ = 0.99
ρ = 0.99
Voriconazole
d
ρ = 1.0
ρ = 0.99
ρ = 0.99
Itraconazole
e
ρ = 0.99
ρ = 0.99
ρ = 0.98
Posaconazole
f
ρ = 0.99
ρ = 0.98
ρ = 0.99
Isavuconazole
g
ρ = 0.99
ρ = 0.99
ρ = 0.99
Clotrimazole
F1
F2
F3
F4

773 **Extended Data Fig. 7 | Correlation between overlapping fragment variants. a,b,c,d,e,f,g,** The fragments of
774 the library had overlapping sequences, which allowed us to assess the reproducibility of the assays by comparing
775 the same variants in different pools of fragments. The selection coefficients are compared among fragments in
776 control (**a**) and in fluconazole (**b**), voriconazole (**c**), itraconazole (**d**), posaconazole (**e**), isavuconazole (**f**) and
777 clotrimazole (**g**). The values are the median selection coefficient of two synonymous codons per amino acid, and
778 in most cases for the median of three replicates. Batch effect for the fragment 4 in the fluconazole condition was
779 corrected with an interpolation model to get new F4 values following a linear regression with F3. Colors represent
780 the different CaErg11 positions in the overlapping regions. Spearman's rank correlation is shown , $P < 0.0001$
781 except when stated otherwise. F1-F2 ; n = 80 amino acid variants, F2-F3 ; n = 60 and F3-F4 ; n = 120.

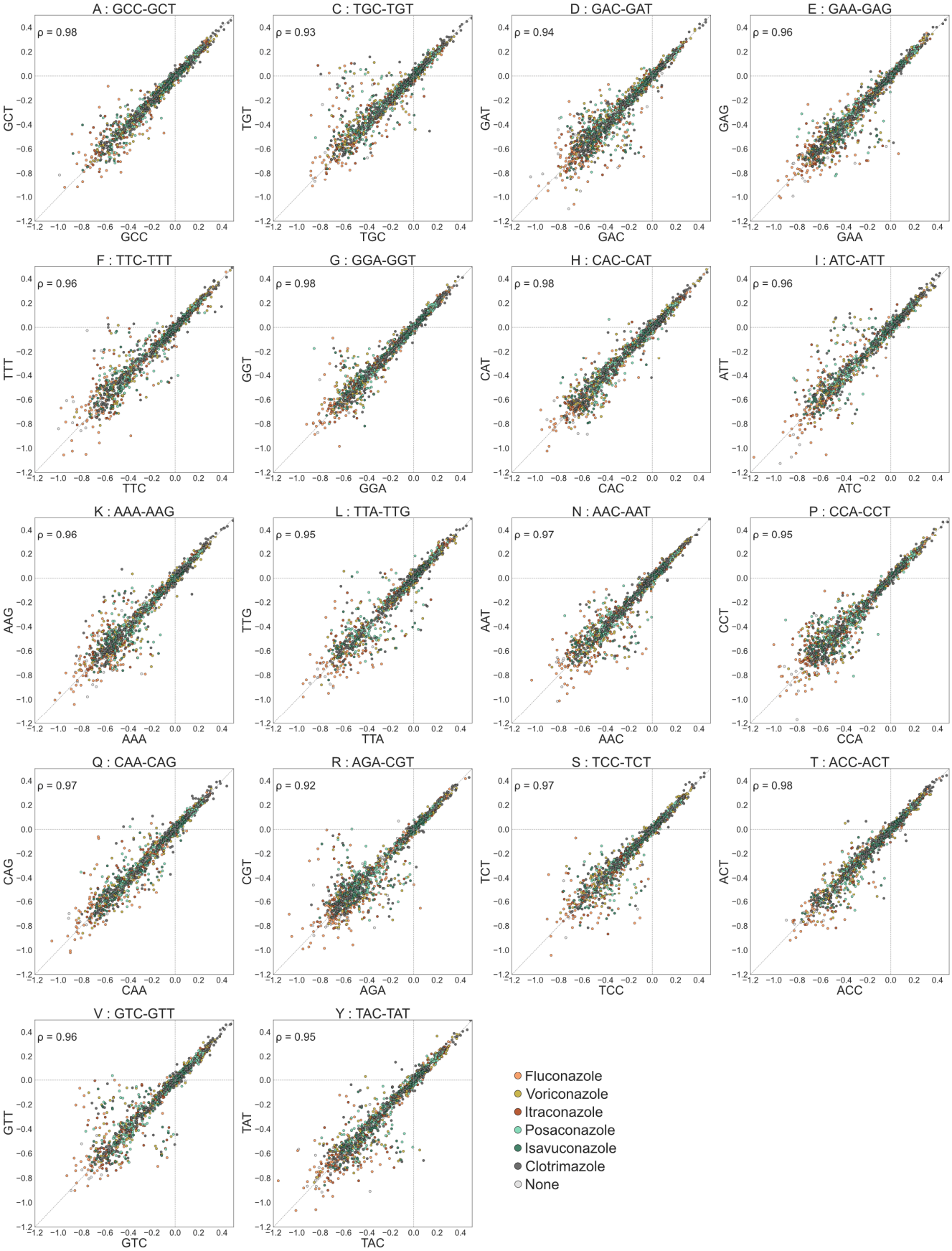
A : GCC-GCT
ρ = 0.98
GCT
GCC
C : TGC-TGT
ρ = 0.93
TGT
TGC
D : GAC-GAT
ρ = 0.94
GAT
GAC
E : GAA-GAG
ρ = 0.96
GAG
GAA
F : TTC-TTT
ρ = 0.96
TTT
TTC
G : GGA-GGT
ρ = 0.98
GGT
GGA
H : CAC-CAT
ρ = 0.98
CAT
CAC
I : ATC-ATT
ρ = 0.96
ATT
ATC
K : AAA-AAG
ρ = 0.96
AAG
AAA
L : TTA-TTG
ρ = 0.95
TTG
TTA
N : AAC-AAT
ρ = 0.97
AAT
AAC
P : CCA-CCT
ρ = 0.95
CCT
CCA
Q : CAA-CAG
ρ = 0.97
CAG
CAA
R : AGA-CGT
ρ = 0.92
CGT
AGA
S : TCC-TCT
ρ = 0.97
TCT
TCC
T : ACC-ACT
ρ = 0.98
ACT
ACC
V : GTC-GTT
ρ = 0.96
GTT
GTC
Y : TAC-TAT
ρ = 0.95
TAT
TAC
Fluconazole
Voriconazole
Itraconazole
Posaconazole
Isavuconazole
Clotrimazole
None

782 **Extended Data Fig. 8 | Correlation between synonymous codons.** In the CaErg11 variant library, each of the
783 206 wild-type residues was replaced with the 19 non-wild type amino acids and this, using two codons when
784 possible. To measure the reproducibility of the results, we looked at the correlation between the selection
785 coefficients of synonymous codons for every amino acid (one letter abbreviation) for the median of three replicates.
786 Colors represent the seven different pooled competition assays. Spearman's rank correlation is shown, $P < 0.0001$.
787 n = 7,448 DNA variants.

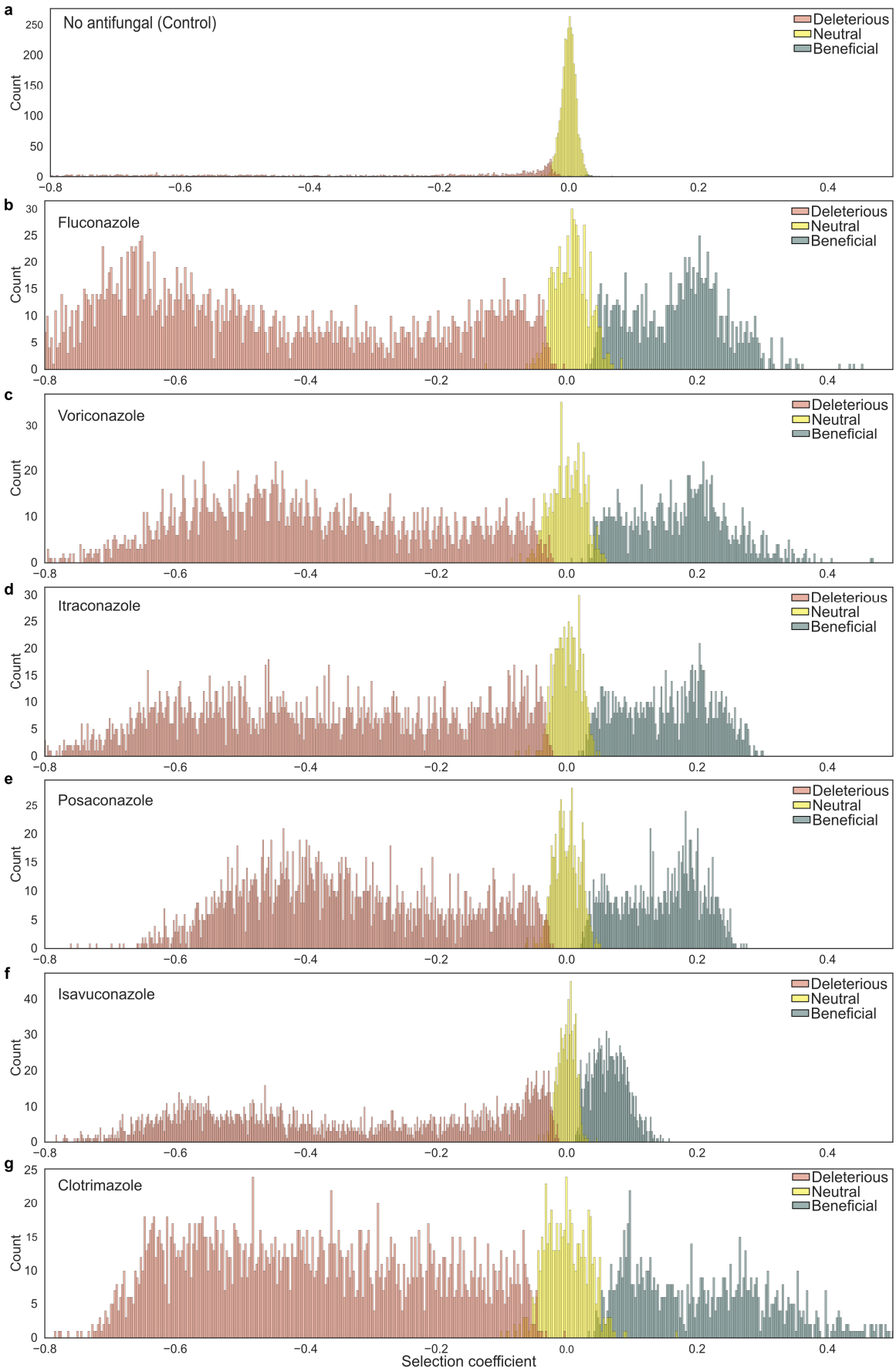
a
No antifungal (Control)
Deleterious
Neutral
Beneficial
Count
b
Fluconazole
c
Voriconazole
d
Itraconazole
e
Posaconazole
f
Isavuconazole
g
Clotrimazole
Selection coefficient

Extended Data Fig. 9 | Distribution of Erg11 variant selection coefficients and their classification. a,b,c,d,e,f,g, Distribution of the selection coefficients in the control condition (**a**) and in fluconazole (**b**), voriconazole (**c**), itraconazole (**d**), posaconazole (**e**), isavuconazole (**f**) and clotrimazole (**g**). Colors represent the different categories. Categories were obtained by comparing the variants with wild-type synonymous codons to missense variants with two-sided independent *t-test* and by correcting *p-values* for multiple comparisons with the Benjamini-Hochberg method (deleterious: $s < 0$ and $P < 0.01$, neutral: $P > 0.01$, beneficial: $s > 0$ and $P < 0.01$). n = 3,830 amino acid variants.

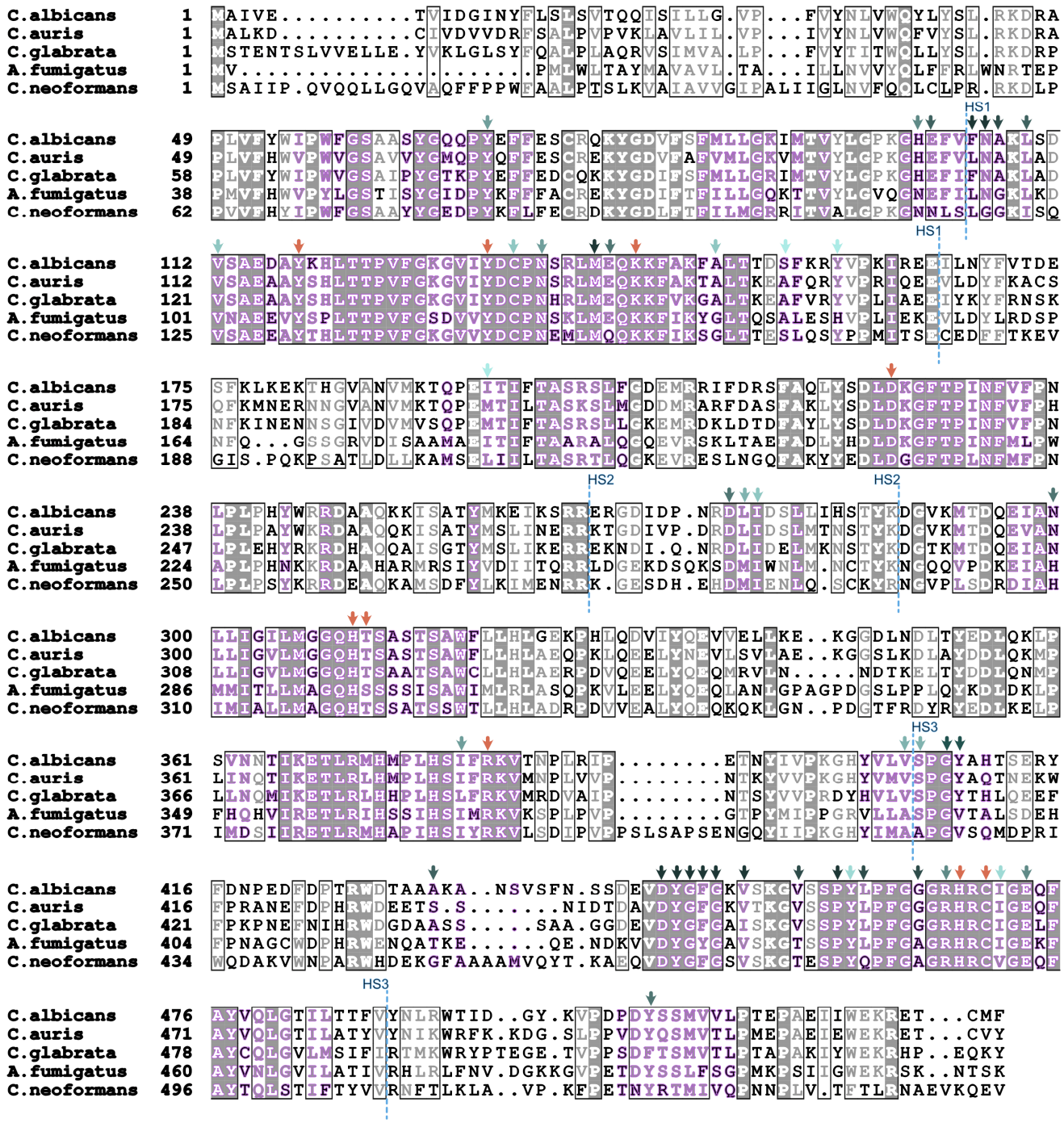

Extended Data Fig. 10 | Multiple sequence alignment of Erg11 from some fungal pathogens. Amino acid positions outlined in purple were included in our CaErg11 library. The orange arrows point to amino acids interacting with the heme (Y118, Y132, K143, R381, H468 and C470) and participating in proton transport to the heme (D225, H310 and T311). Residues with more than 10 variants conferring fluconazole resistance are identified with green arrows (light green: 10/19 aa to dark green: 19/19 aa). They mostly fall into the three resistance clusters (HS) proposed by Marichal *et al.*[51] (in blue, HS1 : 105 to 165, HS2 : 266 to 287 and HS3 : 405 to 488). The alignment was produced using ENDscript 2[50].

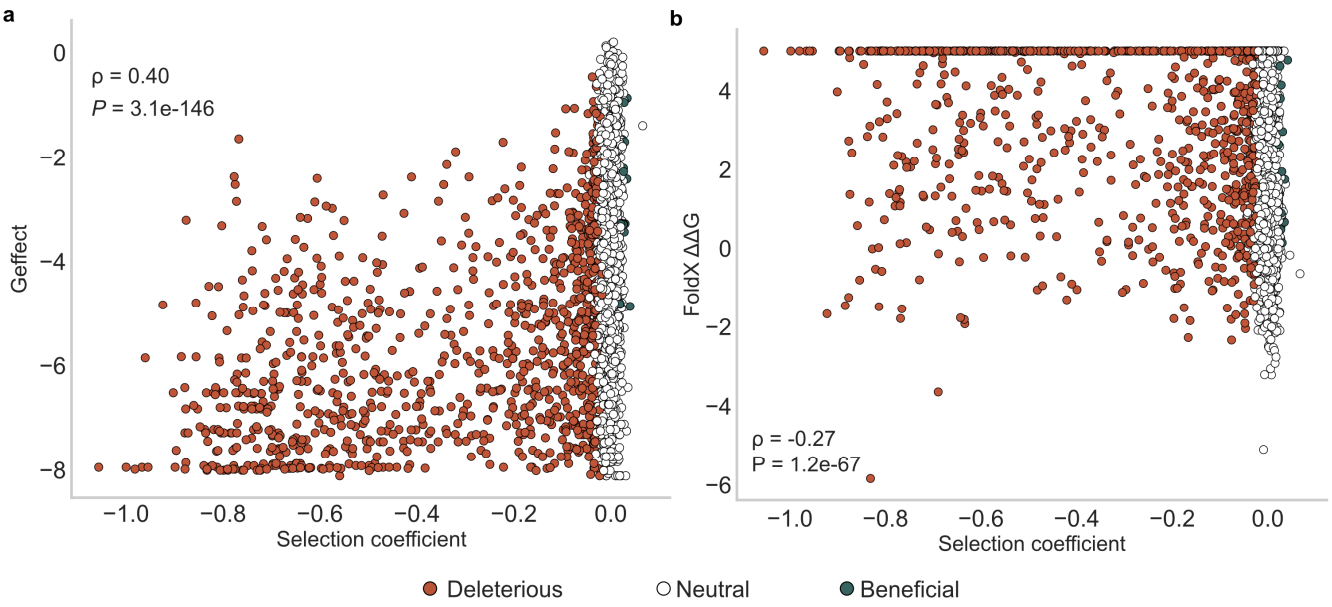

Extended Data Fig. 11 | Estimation of the effect of mutations on the function of Erg11 using an evolutionary model (GEMME) and energy of protein folding modeling (FoldX). a, Relationship between the predicted impact of mutations inferred using long-term evolutionary constraints (Geffect) on Erg11 and selection coefficients in the control condition[48]. GEMME is a computational method that allows prediction of mutational outcomes by modeling the evolutionary history of sequences. Low Geffect values are predicted to be deleterious. Spearman's rank correlation is shown. n = 3,830 amino acid variants. **b,** Examination of the relationship between the prediction of the effects of amino acid substitutions on CaErg11 (PDB ID : 5V5Z) stability from FoldX[49] and the selection coefficient in the control condition. Positive ΔΔG values indicated destabilizing mutations. Spearman's rank correlation is shown. n = 3,830 amino acid variants. The values above ΔΔG of 5 are rounded to 5.

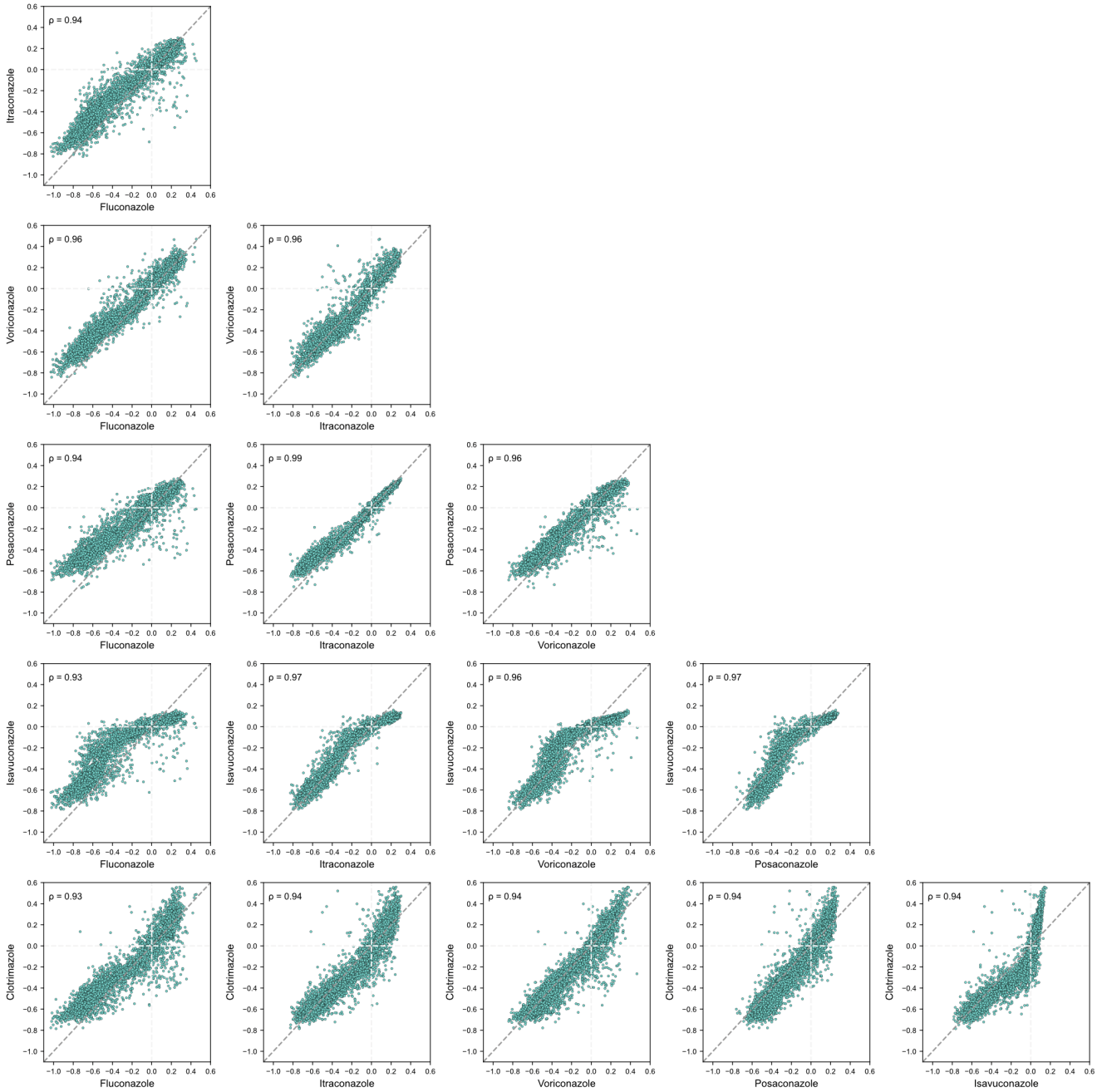

Extended Data Fig. 12 | Correlation between Erg11 variant selection coefficients in the presence of different azoles. Each value is the median of two synonymous codons per amino acid in most cases, and the median of triplicate experimental measurements. Spearman's rank correlation is shown, $P < 0.0001$. n = 3,830 amino acid variants.

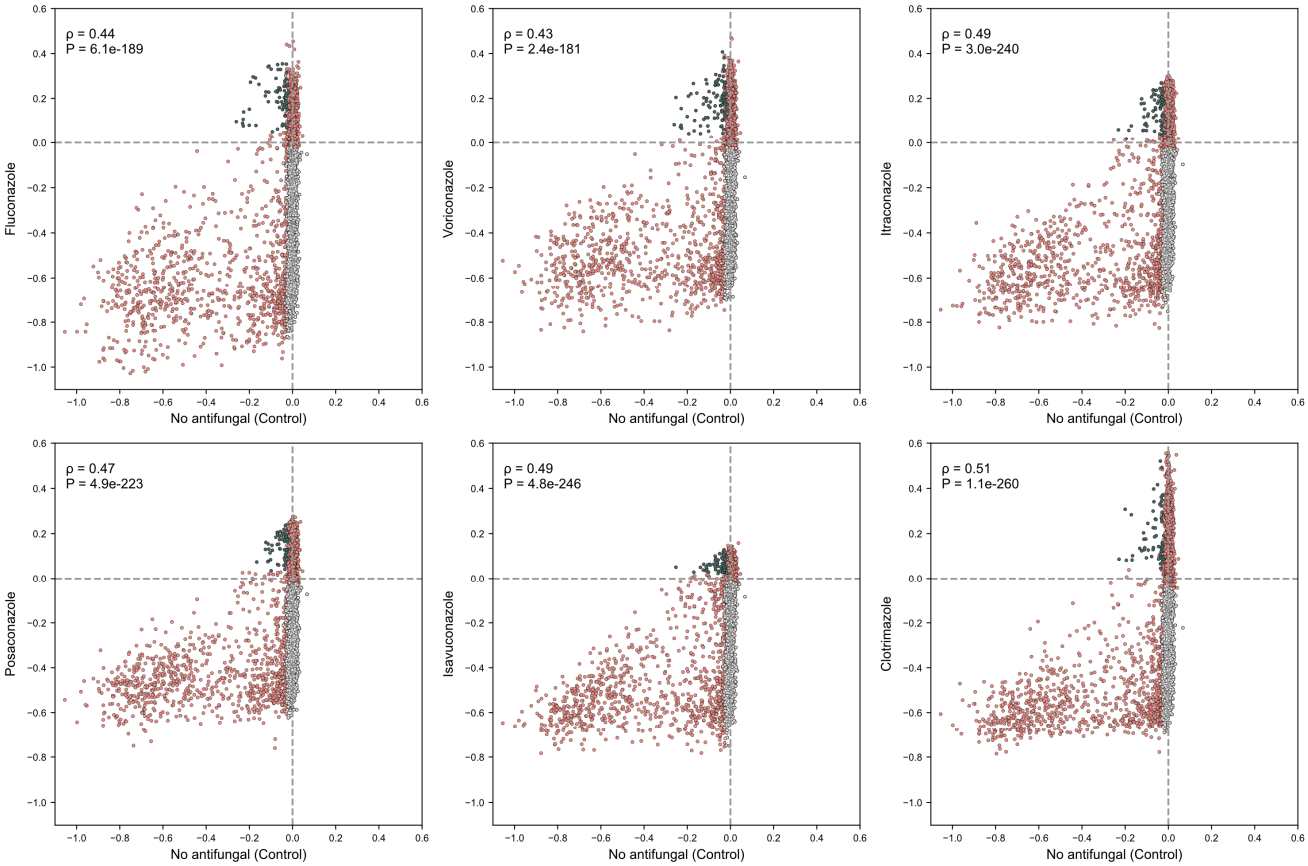

Extended Data Fig. 13 | Correlation between Erg11 variant selection coefficients estimated in azole and in control conditions. Each value is the median of two synonymous codons per amino acid in most cases for the median of triplicate experimental measurements. The dark green dots represent variants with a significant tradeoff, meaning that the mutation is significantly advantageous in azole and deleterious in the control condition. The light grey dots represent deleterious variants in the presence of an azole but not in its absence. Spearman's rank correlation is shown. n = 3,830 amino acid variants.

References

821 1. World Health Organization. Antimicrobial resistance. https://www.who.int/news-room/fact-
822 sheets/detail/antimicrobial-resistance (2023).
823 2. Chapeland-Leclerc, F. *et al.* Acquisition of flucytosine, azole, and caspofungin resistance in Candida
824 glabrata bloodstream isolates serially obtained from a hematopoietic stem cell transplant recipient.
825 *Antimicrob. Agents Chemother.* **54**, 1360–1362 (2010).
826 3. Fisher, M. C. *et al.* Tackling the emerging threat of antifungal resistance to human health. *Nat. Rev.*
827 *Microbiol.* **20**, 557–571 (2022).
828 4. Pappas, P. G., Lionakis, M. S., Arendrup, M. C., Ostrosky-Zeichner, L. & Kullberg, B. J. Invasive
829 candidiasis. *Nat Rev Dis Primers* **4**, 1–20 (2018).
830 5. Pfaller, M. A., Diekema, D. J., Turnidge, J. D., Castanheira, M. & Jones, R. N. Twenty Years of the SENTRY
831 Antifungal Surveillance Program: Results for Candida Species From 1997–2016. *Open Forum Infect. Dis.*
832 **6**, S79–S94 (2019).
833 6. World Health Organisation. WHO fungal priority pathogens list to guide research, development and public
834 health action. https://www.who.int/publications-detail-redirect/9789240060241 (2022).
835 7. Robbins, N., Caplan, T. & Cowen, L. E. Molecular Evolution of Antifungal Drug Resistance. *Annu. Rev.*
836 *Microbiol.* **71**, 753–775 (2017).
837 8. Pappas, P. G. *et al.* Clinical Practice Guideline for the Management of Candidiasis: 2016 Update by the
838 Infectious Diseases Society of America. *Clin. Infect. Dis.* **62**, e1–50 (2016).
839 9. Lee, Y., Robbins, N. & Cowen, L. E. Molecular mechanisms governing antifungal drug resistance. *npj*
840 *Antimicrob Resist* **1**, 1–9 (2023).
841 10. Gow, N. A. R. *et al.* The importance of antimicrobial resistance in medical mycology. *Nat. Commun.* **13**,
842 5352 (2022).
843 11. Arastehfar, A. *et al.* The Quiet and Underappreciated Rise of Drug-Resistant Invasive Fungal Pathogens. *J*
844 *Fungi (Basel)* **6**, (2020).
845 12. Morio, F., Loge, C., Besse, B., Hennequin, C. & Le Pape, P. Screening for amino acid substitutions in the
846 Candida albicans Erg11 protein of azole-susceptible and azole-resistant clinical isolates: new substitutions
847 and a review of the literature. *Diagn. Microbiol. Infect. Dis.* **66**, 373–384 (2010).
848 13. Zhang, J. *et al.* The Fungal CYP51s: Their Functions, Structures, Related Drug Resistance, and Inhibitors.

849 *Front. Microbiol.* **10**, 691 (2019).
850 14. Shelton, J. M. G. *et al.* Citizen science reveals landscape-scale exposures to multiazole-resistant
851 Aspergillus fumigatus bioaerosols. *Science Advances* **9**, eadh8839 (2023).
852 15. Ren, J. *et al.* Fungicides induced triazole-resistance in Aspergillus fumigatus associated with mutations of
853 TR46/Y121F/T289A and its appearance in agricultural fields. *J. Hazard. Mater.* **326**, 54–60 (2017).
854 16. Rhodes, J. *et al.* Population genomics confirms acquisition of drug-resistant Aspergillus fumigatus infection
855 by humans from the environment. *Nat Microbiol* **7**, 663–674 (2022).
856 17. Melnyk, A. H., Wong, A. & Kassen, R. The fitness costs of antibiotic resistance mutations. *Evol. Appl.* **8**,
857 273–283 (2015).
858 18. Vogwill, T. & MacLean, R. C. The genetic basis of the fitness costs of antimicrobial resistance: a meta-
859 analysis approach. *Evol. Appl.* **8**, 284–295 (2015).
860 19. Hawkins, N. J. & Fraaije, B. A. Fitness Penalties in the Evolution of Fungicide Resistance. *Annu. Rev.*
861 *Phytopathol.* **56**, 339–360 (2018).
862 20. Vincent, B. M., Lancaster, A. K., Scherz-Shouval, R., Whitesell, L. & Lindquist, S. Fitness Trade-offs Restrict
863 the Evolution of Resistance to Amphotericin B. *PLoS Biol.* **11**, e1001692 (2013).
864 21. Després, P. C. *et al.* Asymmetrical dose responses shape the evolutionary trade-off between antifungal
865 resistance and nutrient use. *Nat Ecol Evol* 1–15 (2022).
866 22. Ben-Ami, R. *et al.* Fitness and virulence costs of Candida albicans FKS1 hot spot mutations associated with
867 echinocandin resistance. *J. Infect. Dis.* **204**, 626–635 (2011).
868 23. Yang, F. *et al.* The fitness costs and benefits of trisomy of each Candida albicans chromosome. *Genetics*
869 **218**, (2021).
870 24. Sasse, C. *et al.* The stepwise acquisition of fluconazole resistance mutations causes a gradual loss of
871 fitness in Candida albicans. *Mol. Microbiol.* **86**, 539–556 (2012).
872 25. Valsecchi, I., Mellado, E., Beau, R., Raj, S. & Latgé, J.-P. Fitness Studies of Azole-Resistant Strains of
873 Aspergillus fumigatus. *Antimicrob. Agents Chemother.* **59**, 7866–7869 (2015).
874 26. Jacobs, S. E. *et al.* Candida auris Pan-Drug-Resistant to Four Classes of Antifungal Agents. *Antimicrob.*
875 *Agents Chemother.* **0**, e00053–22 (2022).
876 27. Madrazo-Moya, C. F. *et al.* Whole genomic sequencing as a tool for diagnosis of drug and multidrug-
877 resistance tuberculosis in an endemic region in Mexico. *PLoS One* **14**, e0213046 (2019).

878 28. Alastruey-Izquierdo, A. & Martín-Galiano, A. J. The challenges of the genome-based identification of
879 antifungal resistance in the clinical routine. *Front. Microbiol.* **14**, 1134755 (2023).
880 29. Dewachter, L. *et al.* Deep mutational scanning of essential bacterial proteins can guide antibiotic
881 development. *Nat. Commun.* **14**, 241 (2023).
882 30. Butts, A., Palmer, G. E. & Rogers, P. D. Antifungal adjuvants: Preserving and extending the antifungal
883 arsenal. *Virulence* **8**, 198–210 (2017).
884 31. Uthayakumar, D., Sharma, J., Wensing, L. & Shapiro, R. S. CRISPR-Based Genetic Manipulation of
885 Candida Species: Historical Perspectives and Current Approaches. *Frontiers in Genome Editing* **2**, (2021).
886 32. Albarrag, A. M. *et al.* Interrogation of Related Clinical Pan-Azole-Resistant Aspergillus fumigatus Strains:
887 G138C, Y431C, and G434C Single Nucleotide Polymorphisms in cyp51A, Upregulation of cyp51A, and
888 Integration and Activation of Transposon Atf1 in the cyp51A Promoter. *Antimicrob. Agents Chemother.* **55**,
889 5113–5121 (2011).
890 33. Alcazar-Fuoli, L., Mellado, E., Cuenca-Estrella, M. & Sanglard, D. Probing the role of point mutations in the
891 cyp51A gene from Aspergillus fumigatus in the model yeast Saccharomyces cerevisiae. *Med. Mycol.* **49**,
892 276–284 (2011).
893 34. Carter, H. E. *et al.* Alterations in the predicted regulatory and coding regions of the sterol 14α-demethylase
894 gene (CYP51) confer decreased azole sensitivity in the oilseed rape pathogen Pyrenopeziza brassicae.
895 *Mol. Plant Pathol.* **15**, 513–522 (2014).
896 35. Healey, K. R. & Singh, A. Heterologous Expression of Candida Antifungal Target Genes in the Model
897 Organism Saccharomyces cerevisiae. in *Antifungal Drug Resistance: Methods and Protocols* (eds. Krysan,
898 D. J. & Moye-Rowley, W. S.) 181–190 (Springer US, 2023).
899 36. Hull, C. M. *et al.* Facultative Sterol Uptake in an Ergosterol-Deficient Clinical Isolate of Candida glabrata
900 Harboring a Missense Mutation in ERG11 and Exhibiting Cross-Resistance to Azoles and Amphotericin B.
901 *Antimicrob. Agents Chemother.* **56**, 4223–4232 (2012-8).
902 37. Wu, Y., Gao, N., Li, C., Gao, J. & Ying, C. A newly identified amino acid substitution T123I in the 14α-
903 demethylase (Erg11p) of Candida albicans confers azole resistance. *FEMS Yeast Res.* **17**, (2017).
904 38. Xiang, M.-J. *et al.* Erg11 mutations associated with azole resistance in clinical isolates of Candida albicans.
905 *FEMS Yeast Res.* **13**, 386–393 (2013).
906 39. Mnaimneh, S. *et al.* Exploration of Essential Gene Functions via Titratable Promoter Alleles. *Cell* **118**, 31–44

907 (2004).
908 40. Keniya, M. V. *et al.* Crystal Structures of Full-Length Lanosterol 14α-Demethylases of Prominent Fungal
909 Pathogens Candida albicans and Candida glabrata Provide Tools for Antifungal Discovery. *Antimicrob.*
910 *Agents Chemother.* **62**, (11 2018).
911 41. Flowers, S. A., Colón, B., Whaley, S. G., Schuler, M. A. & Rogers, P. D. Contribution of Clinically Derived
912 Mutations in ERG11 to Azole Resistance in Candida albicans. *Antimicrob. Agents Chemother.* **59**, 450–460
913 (2015).
914 42. Warrilow, A. G. *et al.* The Evolution of Azole Resistance in Candida albicans Sterol 14α-Demethylase
915 (CYP51) through Incremental Amino Acid Substitutions. *Antimicrob. Agents Chemother.* **63**, e02586–18
916 (2019).
917 43. Alvarez-Rueda, N. *et al.* Amino acid substitutions at the major insertion loop of Candida albicans sterol
918 14alpha-demethylase are involved in fluconazole resistance. *PLoS One* **6**, e21239 (2011).
919 44. Accoceberry, I. *et al.* A CTG Clade Candida Yeast Genetically Engineered for the Genotype-Phenotype
920 Characterization of Azole Antifungal Resistance in Human-Pathogenic Yeasts. *Antimicrob. Agents*
921 *Chemother.* **62**, (2018).
922 45. Allen, D., Wilson, D., Drew, R. & Perfect, J. Azole antifungals: 35 years of invasive fungal infection
923 management. *Expert Rev. Anti. Infect. Ther.* **13**, 787–798 (2015).
924 46. Kim, S. *et al.* PubChem 2023 update. *Nucleic Acids Res.* **51**, D1373–D1380 (2023).
925 47. Hargrove, T. Y. *et al.* Structural analyses of Candida albicans sterol 14α-demethylase complexed with azole
926 drugs address the molecular basis of azole-mediated inhibition of fungal sterol biosynthesis. *J. Biol. Chem.*
927 **292**, 6728–6743 (2017).
928 48. Laine, E., Karami, Y. & Carbone, A. GEMME: A Simple and Fast Global Epistatic Model Predicting
929 Mutational Effects. *Mol. Biol. Evol.* **36**, 2604–2619 (2019).
930 49. Schymkowitz, J. *et al.* The FoldX web server: an online force field. *Nucleic Acids Res.* **33**, W382–8 (2005).
931 50. Robert, X. & Gouet, P. Deciphering key features in protein structures with the new ENDscript server. *Nucleic*
932 *Acids Res.* **42**, W320–4 (2014).
933 51. Marichal, P. *et al.* Contribution of mutations in the cytochrome P450 14α-demethylase (Erg11p, Cyp51p) to
934 azole resistance in Candida albicans. *Microbiology* **145**, 2701–2713 (1999).
935 52. Ford, C. B. *et al.* The evolution of drug resistance in clinical isolates of Candida albicans. *Elife* **4**, e00662

936 (2015).
937 53. Verweij, P. E. *et al.* In-host adaptation and acquired triazole resistance in Aspergillus fumigatus: a dilemma
938 for clinical management. *Lancet Infect. Dis.* **16**, e251–e260 (2016).
939 54. Hinz, A., Amado, A., Kassen, R., Bank, C. & Wong, A. Unpredictability of the fitness effects of antimicrobial
940 resistance mutations across environments in Escherichia coli. Preprint at
941 https://doi.org/10.1101/2023.10.25.563906 (2023).
942 55. Fisher, M. C. *et al.* Threats Posed by the Fungal Kingdom to Humans, Wildlife, and Agriculture. *MBio* **11**,
943 e00449–20 (2020).
944 56. Lockhart, S. R., Chowdhary, A. & Gold, J. A. W. The rapid emergence of antifungal-resistant human-
945 pathogenic fungi. *Nat. Rev. Microbiol.* 1–15 (2023).
946 57. Li, J. *et al.* Novel ERG11 and TAC1b Mutations Associated with Azole Resistance in Candida auris.
947 *Antimicrob. Agents Chemother.* **65**, 10.1128/aac.02663–20 (2021).
948 58. Williamson, B. *et al.* Impact of Erg11 Amino Acid Substitutions Identified in Candida auris Clade III Isolates
949 on Triazole Drug Susceptibility. *Antimicrob. Agents Chemother.* **66**, e0162421 (2022).
950 59. Sagatova, A. A., Keniya, M. V., Tyndall, J. D. A. & Monk, B. C. Impact of Homologous Resistance Mutations
951 from Pathogenic Yeast on Saccharomyces cerevisiae Lanosterol 14α-Demethylase. *Antimicrob. Agents*
952 *Chemother.* **62**, e02242–17 (2018).
953 60. Kang, S. E. *et al.* Evidence for the agricultural origin of resistance to multiple antimicrobials in Aspergillus
954 fumigatus, a fungal pathogen of humans. *G3 Genes|Genomes|Genetics* **12**, jkab427 (2022).
955 61. Snelders, E. *et al.* Triazole Fungicides Can Induce Cross-Resistance to Medical Triazoles in Aspergillus
956 fumigatus. *PLoS One* **7**, e31801 (2012).
957 62. Verweij, P. E. *et al.* Dual use of antifungals in medicine and agriculture: How do we help prevent resistance
958 developing in human pathogens? *Drug Resist. Updat.* **65**, 100885 (2022).
959 63. Bastos, R. W., Rossato, L., Goldman, G. H. & Santos, D. A. Fungicide effects on human fungal pathogens:
960 Cross-resistance to medical drugs and beyond. *PLoS Pathog.* **17**, e1010073 (2021).
961 64. Castelo-Branco, D. *et al.* Collateral consequences of agricultural fungicides on pathogenic yeasts: A One
962 Health perspective to tackle azole resistance. *Mycoses* **65**, 303–311 (2022).
963 65. Hughes, T. R. *et al.* Functional discovery via a compendium of expression profiles. *Cell* **102**, 109–126
964 (2000).

965 66. Gillum, A. M., Tsay, E. Y. H. & Kirsch, D. R. Isolation of the Candida albicans gene for orotidine-5′-
966 phosphate decarboxylase by complementation of S. cerevisiae ura3 and E. coli pyrF mutations. *Mol. Gen.*
967 *Genet.* **198**, 179–182 (1984).
968 67. Gibson, D. G. *et al.* Enzymatic assembly of DNA molecules up to several hundred kilobases. *Nat. Methods*
969 **6**, 343–345 (2009).
970 68. Hénault, M., Marsit, S., Charron, G. & Landry, C. R. The genomic landscape of transposable elements in
971 yeast hybrids is shaped by structural variation and genotype-specific modulation of transposition rate.
972 Preprint at https://doi.org/10.1101/2023.05.08.539935 (2023).
973 69. Ho, C. H. *et al.* A molecular barcoded yeast ORF library enables mode-of-action analysis of bioactive
974 compounds. *Nat. Biotechnol.* **27**, 369–377 (2009).
975 70. Santos, M. A. & Tuite, M. F. The CUG codon is decoded in vivo as serine and not leucine in Candida
976 albicans. *Nucleic Acids Res.* **23**, 1481–1486 (1995).
977 71. Evans-Yamamoto, D. *et al.* Parallel nonfunctionalization of CK1δ/ε kinase ohnologs following a whole-
978 genome duplication event. Preprint at https://doi.org/10.1101/2023.10.02.560513 (2023).
979 72. Gietz, R. D. & Schiestl, R. H. High-efficiency yeast transformation using the LiAc/SS carrier DNA/PEG
980 method. *Nat. Protoc.* **2**, 31–34 (2007).
981 73. Durand, R., Jalbert-Ross, J., Fijarczyk, A., Dubé, A. K. & Landry, C. R. Cross-feeding affects the target of
982 resistance evolution to an antifungal drug. *PLoS Genet.* **19**, e1011002 (2023).
983 74. Nash, A. *et al.* MARDy: Mycology Antifungal Resistance Database. *Bioinformatics* **34**, 3233–3234 (2018).
984 75. Cock, P. J. A. *et al.* Biopython: freely available Python tools for computational molecular biology and
985 bioinformatics. *Bioinformatics* **25**, 1422–1423 (2009).
986 76. Starr, T. N. *et al.* Deep Mutational Scanning of SARS-CoV-2 Receptor Binding Domain Reveals Constraints
987 on Folding and ACE2 Binding. *Cell* **182**, 1295–1310.e20 (2020).
988 77. Andrews, S. FastQC: A Quality Control Tool for High Throughput Sequence Data. Available online at:
989 https://www.bioinformatics.babraham.ac.uk/projects/fastqc/ (2010).
990 78. Masella, A. P., Bartram, A. K., Truszkowski, J. M., Brown, D. G. & Neufeld, J. D. PANDAseq: paired-end
991 assembler for illumina sequences. *BMC Bioinformatics* **13**, 31 (2012).
992 79. Rognes, T., Flouri, T., Nichols, B., Quince, C. & Mahé, F. VSEARCH: a versatile open source tool for
993 metagenomics. *PeerJ* **4**, e2584 (2016).

994 80. Rice, P., Longden, I. & Bleasby, A. EMBOSS: The European Molecular Biology Open Software Suite.
995 *Trends Genet.* **16**, 276–277 (2000).
996 81. Cisneros, A. F. *et al.* Epistasis between promoter activity and coding mutations shapes gene evolvability.
997 *Science Advances* **9**, eadd9109 (2023).
998 82. Shapiro, R. S. *et al.* A CRISPR-Cas9-based gene drive platform for genetic interaction analysis in Candida
999 albicans. *Nat Microbiol* **3**, 73–82 (2018).
1000 83. Razzaq, I. *et al.* The SAGA and NuA4 component Tra1 regulates Candida albicans drug resistance and
1001 pathogenesis. *Genetics* **219**, (2021).
1002 84. Peng, D. & Tarleton, R. EuPaGDT: a web tool tailored to design CRISPR guide RNAs for eukaryotic
1003 pathogens. *Microb Genom* **1**, e000033 (2015).
1004 85. Wensing, L. *et al.* A CRISPR Interference Platform for Efficient Genetic Repression in Candida albicans.
1005 *mSphere* **4**, 10.1128/msphere.00002–19 (2019).
1006 86. Mirdita, M. *et al.* ColabFold: making protein folding accessible to all. *Nat. Methods* **19**, 679–682 (2022).
1007 87. Tiberti, M. *et al.* MutateX: an automated pipeline for in silico saturation mutagenesis of protein structures
1008 and structural ensembles. *Brief. Bioinform.* **23**, (2022).
1009 88. Delgado, J., Radusky, L. G., Cianferoni, D. & Serrano, L. FoldX 5.0: working with RNA, small molecules and
1010 a new graphical interface. *Bioinformatics* **35**, 4168–4169 (2019).
1011 89. Radusky, L. G. & Serrano, L. pyFoldX: enabling biomolecular analysis and engineering along structural
1012 ensembles. *Bioinformatics* **38**, 2353–2355 (2022).
1013 90. Meng, E. C. *et al.* UCSF ChimeraX: Tools for structure building and analysis. *Protein Sci.* **32**, e4792 (2023).
1014 91. Hunter, J. D. Matplotlib: A 2D Graphics Environment. *Comput. Sci. Eng.* **9**, 90–95 (2007).
1015 92. Harris, C. R. *et al.* Array programming with NumPy. *Nature* **585**, 357–362 (2020).
1016 93. Lex, A., Gehlenborg, N., Strobelt, H., Vuillemot, R. & Pfister, H. UpSet: Visualization of Intersecting Sets.
1017 *IEEE Trans. Vis. Comput. Graph.* **20**, 1983–1992 (2014).
1018 94. Virtanen, P. *et al.* SciPy 1.0: fundamental algorithms for scientific computing in Python. *Nat. Methods* **17**,
1019 261–272 (2020).
1020 95. The pandas development team. pandas-dev/pandas: Pandas . *Zenodo* (2022).
1021 96. Waskom, M. L. seaborn: statistical data visualization. *Journal of Open Source Software* **6**, 3021 (2021).